Water-soluble, heterometallic chalcogenide oligomers as building blocks for functional films

Jean-Yves Chane-Ching, Lionel Perrin, Pascal Puech, Valérie Bourdon, Vincent Foncrose, Andrea Balocchi, Xavier Marie, Pierre Lavedan

Water-soluble, heterometallic chalcogenide oligomers as building blocks for functional films†

J. Y. Chane Ching,*[a] L. Perrin,[b] P. Puech,[c] V. Bourdon,[d] V. Foncrose,[a] A. Balocchi,[e] X. Marie[e] and P. Lavedan[d]

Monometallic chalcogenide aqueous complexes such as $(Sn_2S_6)^{4-}$ and $(Sn_4S_{10})^{4-}$ are widely used as functional ligands with applications in nano-electronics and solar cells. We propose a general process route to the formation of all-inorganic, heterometallic chalcogenide oligomers, thus expanding the range of these functional aqueous ligands. From electrospray ionization mass spectrometry, tetramers were shown to be the most predominant oligomers synthesized in Sn(IV)–Zn(II)–S(II), Sn(IV)–Zn(II)–Se(II) and Sn(IV)–Ga(III)–S(II) systems. While tetramers possessing exclusively one Zn cation were identified in the Sn(IV)–Zn(II)–S(II) system, the full range of solid solutions was achieved for $(Sn_a–Ga_b–S_c)^{t-}$ oligomers with $1 \leq a \leq 4$. Using *in situ* characterization by ^{119}Sn liquid NMR and Raman spectroscopy, supported by DFT calculations, we demonstrate that the various tetramers adopt a compact adamantane-like structure. The charge of the heterometallic oligomers was shown to be controlled by the doping cation valence and the chalcogenide anion deficiency in the tetramers. These water-soluble heterometallic chalcogenide oligomers can serve as ligands, residue-free dispersants or building blocks for functional film fabrication. Using these oligomers, we report here the fabrication of chalcogenide solar cells employing environmentally friendly, all-aqueous, $(Sn_a–Zn_b–S_c)^{t-}$-capped CZTS nanocrystal inks.

DOI: 10.1039/c5qi00250h

Introduction

Soluble metal chalcogenide complexes represent exciting building blocks largely used in various applications such as nanoelectronics,[1,2] photovoltaics[3] or thermoelectrics.[4–6] The use of hydrazinium soluble complexes for semiconducting films was first introduced by Mitzi *et al.*[1] Indeed, the clean temperature decomposition of these precursors yields ultra-thin (50 Å), crystalline and continuous metal chalcogenide films for nanoelectronics. Used as electronic linkers, these soluble complexes have been proven to increase electron mobility in nanocrystal arrays, allowing semiconductors to be patterned onto large area substrates for photovoltaics or thermoelectrics.[7] More recently, the number of these hydrazinium metal chalcogenide complexes has been increasing. A general synthetic route involving the use of an alkali metal hydride was proposed[8] for dissolving a number of metal chalcogenides previously considered to be unreactive. Availability of new complexes such as $CdTe^{2-}$, $Cd_2Se_3^{2-}$, $PbTe_2^{2-}$, and $Bi_2Te_5^{4-}$ has allowed achieving excellent electron mobility in nanocrystal semiconductor films, widely used in photovoltaics and thermo-electrics. Another strategy is to develop hydrazinium-free, water-soluble, environmentally friendly metal chalcogenide precursors. These water-soluble metal chalcogenide oligomers can be associated with NH_4^+ counterions to yield highly pure films. While many metal chalcogenide clusters were previously synthesized with an emphasis on the use of organic cations as structure-directing agents,[9,10] purely inorganic, hydrazinium-free chalcogenide systems have received less attention. Pioneering studies by Krebs[11–15] described isolated water-soluble $(Sn_2S_6)^4$, $(Sn_4Se_{10})^{4-}$, and $(Ga_4Se_{10})^{8-}$ chalcogenide complexes with Na^+ as the counterion. The reported complexes, usually composed of two or four metal centers of the same metallic cation, were largely developed as ligands for improved electrostatic colloidal stabilization[16] or enhanced electronic coupling.[17]

Here, we propose to expand the list of these water-soluble, all-inorganic complexes to heterometallic chalcogenide oligomers. Indeed, association of metal cations that display various valences in a single metal chalcogenide oligomer can

[a]*Université de Toulouse, UPS, CNRS, CIRIMAT, 118 Route de Narbonne, F 31062 Toulouse, France. E mail: chane@chimie.ups tlse.fr*

[b]*Université de Lyon 1, Claude Bernard, ICBMS, UMR 5246, CNRS, INSA, CPE 43 Bd du 11 nov 1918, 69622 Villeurbanne cedex, France*

[c]*Université de Toulouse, CNRS, CEMES, 29 rue Jeanne Marvig, 31055 Toulouse, France*

[d]*Université de Toulouse, UPS, Service commun, 118 Route de Narbonne, F 31062 Toulouse, France*

[e]*Université de Toulouse, INSA CNRS UPS, LPCNO, 135 Av. Rangueil, 31077 Toulouse, France*

†Electronic supplementary information (ESI) available. See DOI: 10.1039/c5qi00250h

improve their electronic and thermal conduction. In addition, their large-scale use in numerous applications such as thermoelectrics and photovoltaics will be facilitated if they are cheap and simple. A nice platform suited to the integration of these heterometallic chalcogenide oligomers is earth abundant copper–zinc–tin chalcogenide ($Cu_2ZnSnSSe_4$, CZTSSe) thin films. These films have recently attracted increasing attention[18–21] as absorbers for low-cost solar cells. Indeed, solution-based deposition routes[22,23] have been recently proposed to potentially provide low-cost scalable routes for the fabrication of CZTSSe solar cells. While solution-based process routes currently involve hydrazine[22] or hexane-thiol[23] as solvents, less toxic[24,25] or safer process routes involving green, stable, all-aqueous inks[26] were recently reported for the fabrication of CZTS solar cells. To produce all-aqueous inks, tin chalcogenide complexes including $Sn_2S_6^{4-}$ and $Sn_2S_7^{6-}$ were proposed as ligands to *in situ* cap the Cu/Zn sulfide nanoparticles,[26] resulting in homogeneous and stable dispersions for the formation of CZTS,Se films. Another environmentally friendly approach was developed in our group involving a high temperature nanocrystal synthetic route[27] producing low electronic-defect concentration Cu_2ZnSnS_4 (CZTS) building blocks. The surfaces of these CZTS nanocrystals were further purified by S^{2-} exchange, yielding deagglomerated Cu_2ZnSnS_4 nanocrystal dispersions. Hence, the design and synthesis of suitable ligands are key steps in the fabrication of high performance films.[28] In this context, expanding the range of water-soluble, all-inorganic, highly electrostatically charged metal chalcogenide oligomers represents an interesting challenge. In particular, heterometallic chalcogenide oligomers should be of great interest since they could allow both a better nanocrystal surface charge control and a homogeneous fine-tuning of the nanocrystal film composition. Because of the high potentiality of the CZTSSe solar cell as a low-cost solar cell,[18] we focus on the design and synthesis of $(Sn_a–Zn_b–S_c)^{t-}$ oligomers. Indeed, Sn and Zn cations over-stoichiometries are required for the fabrication of high performance CZTSSe solar cells,[22] rendering $(Sn_a–Zn_b–S_c)^{t-}$ oligomers very attractive as all-inorganic dispersants for the design of high purity CZTS dispersions. Heterometallic $(Sn_a–Ga_b–S_c)^{t-}$ oligomers including Ga(III) were also explored. We selected Ga(III) as a model trivalent dopant capable of promoting the electronic conductivity of CZTS[29] for thermoelectric applications.

A general method for the synthesis of highly water-soluble, discrete, heterometallic, chalcogenide oligomers is proposed involving a facile, low-cost process route and ammonium as the residue-free counterion. Our strategy is based on the incorporation, under mild conditions, of a high-valent cation, introducing stacking faults or symmetry loss into the chalcogenide framework, resulting in lower molecular mass, highly water-soluble oligomers. The chemical composition of the oligomers was determined by electrospray ionization mass spectrometry, demonstrating their heterometallic character. The structure of the oligomers was probed by liquid ^{119}Sn NMR and Raman spectroscopy and supported by quantum chemical calculations at the DFT level. These heterometallic chalcogenide oligomers could prove effective as building blocks for the design of an aqueous, environmentally friendly process route to the fabrication of Cu_2ZnSnS,Se_4 (CZTS,Se) solar cells. We will show that these building blocks can serve as highly charged, all-inorganic, aqueous ligands. Preliminary results describing a solar cell fabricated from an all-aqueous, $(Sn_a–Zn_b–S_c)^{t-}$ capped CZTS nanocrystal dispersion and displaying an encouraging efficiency of 2.6% are reported.

Experimental section

Chemicals

$(NH_4)_2S$ (solution, 20% d = 1.1 Sigma Aldrich), $ZnCl_2$ (Sigma), $SnCl_4$ $5H_2O$ (Fisher Chemicals), $CH_3NaO_3S{\cdot}xH_2O$ (or hydroxymethanesulfinate hydrate or Rongalite, Aldrich) and Se metal (Acros) were used as received. $GaCl_3$ solution was prepared by dissolution of Ga_2O_3 (99.99%, Rhodia) in 6 M HCl in an autogeneous reactor at 200 °C for 16 h.

Heterometallic chalcogenide oligomer synthesis

Two main process routes have been proposed[11,12] for the synthesis of water-soluble chalcogenide oligomers. The first route involves the metal sulfide dissolution in highly basic sulfide solution. In the second route, the oligomers are formed from homogeneous ionic solutions. Because the metal sulfide dissolution process involves highly basic pH, we have explored the formation of heterometallic chalcogenide oligomers from homogeneous solutions since this route allows investigation of larger $[S^{2-}]$ and pH ranges. Oligomers were prepared from solutions defined by two key parameters, s and h (or oh), $s = [S^{2-}]/\sum[M]$, $h = [H^+]/\sum[M]$, and (oh) $= [OH^-]/\sum[M]$, with M = Sn (IV) or Zn(II) or Ga(III).

Experimental procedure for the preparation of $(Sn_a–Zn_b–S_c)^{t-}$ oligomers. Typically, a solution containing Sn^{4+} and Zn^{2+} cations was prepared by dissolution of 4.7 g (13.33 mmol) of $SnCl_4$ 5 H_2O and 0.912 g (6.66 mmol) of $ZnCl_2$ into 100 mL 0.1 M HCL ($H^+/([Zn] + [Sn]) = 0.5$). 100 mL of ammonium sulfide solution was prepared by dilution of 37.15 mL of 3.23 M (20% $(NH_4)_2S$) commercial solution using deionized H_2O. $(Sn_a–Zn_b–S_c)^{t-}$ oligomer solution was prepared by instantaneous addition of the metal cation solution into the $(NH_4)_2S$ solution at room temperature under vigorous stirring. The oligomer solution ($x_{Zn} = [Zn]/([Sn] + [Zn]) = 0.33$, $([Sn] + [Zn]) = 0.1$ M, $s = [S^{2-}]/([Sn] + [Zn]) = 6$) became limpid after one hour.

Preparation of $(Sn_a–Ga_b–S_c)^{t-}$ oligomers. Similarly, a solution containing Sn^{4+} and Ga^{3+} cations was prepared by dissolution of 1.75 g (5 mmol) of $SnCl_4$ $5H_2O$ into 6.25 mL (5 mmol) of 0.8 M $GaCl_3$ solution and made up to a final volume of 25 mL. This metal cation solution was added to 25 mL of ammonium sulfide solution, prepared by dilution of 18.55 mL of 3.23 M (20% $(NH_4)_2S$) commercial solution. A limpid $(Sn_a–Ga_b–S_c)^{t-}$ oligomer solution ($x_{Ga} = [Ga]/([Sn] + [Ga]) = 0.50$, $([Sn] + [Ga]) = 0.2$ M, $s = [S^{2-}]/([Sn] + [Ga]) = 6$) was obtained by the instantaneous addition of the solution containing the

metal cations into the $(NH_4)_2S$ solution and then stirring overnight.

Preparation of $(Sn_a–Zn_b–Se_c)^{t-}$ oligomers. The $(NH_4)_2Se$ solution was prepared by reduction of Se metal using $CH_3NaO_3S{\cdot}xH_2O$ (Rongalite) as a reducing agent under a N_2 atmosphere. Typically, 5.70 g Rongalite was dissolved into a 4 M NH_3 solution. Then 20 mmol of Se (1.58 g Se) were added into the as-prepared basic solution. Once the Se was completely dissolved, a solution containing Sn^{4+} and Zn^{2+} cations ($[H^+]/([Sn^{4+}] + [Zn^{2+}]) = 0.5$, $x_{Zn} = 0.5$) was instantaneously added to the freshly prepared $(NH_4)_2Se$ solution. The final concentrations of the (NH_4^+) $(Sn_a–Zn_b–Se_c)^{t-}$ oligomers were ([Sn] + [Zn]) = 0.1 M and [Se]/([Zn] + [Sn]) = 3. *Caution: Se^{2-} solutions must be handled avoiding acidic pH to prevent the formation of highly toxic H_2Se.*

Oligomers characterization

While the identification of metal chalcogenide solid clusters is generally performed by single-crystal X-ray diffraction, large broad peaks were recorded by X-ray investigation on precipitated solid oligomers. Insights into the speciation of solution species and the structure of the oligomers were gained using *in situ* liquid techniques including electrospray ionization mass spectrometry (ESI-MS), Dynamic Light Scattering (DLS), and Raman and NMR spectroscopy.

Electrospray ionization mass spectrometry (ESI-MS). ESI-MS data were collected using a Xevo G2 Q Tof MS instrument equipped with an electrospray (ESI) source supplied by Waters. The detector is an electron multiplier and all the data were processed using the Masslynx 4.1 software. 1 μl of the sample was introduced into the MS using flow injection analysis. The electrospray source was used at a drying nitrogen gas temperature of approx. +100 °C. Because ionization processes induce fragmentation, careful optimization of the experimental conditions was performed for the speciation chemistry in solution. ESI parameters used in each data ESI-MS collection are cone voltage = 30 V and time of acquisition = 2 min. All the MS data were collected in negative ion mode on the as-synthesized solutions (0.1 M ([Sn] + [Zn]) or 0.1 M ([Sn] + [Ga])) without any dilution. The spectrometer was calibrated to give a precision of 3.0 ppm in the region 100–2000 *m*/*z*. In the following, experimentally identified species are reported in the figures. Note that these species are often protonated. Because this protonation can arise from either the gas phase protonation in the mass spectrometry chamber or the slightly basic pH of the solutions, these species will be mentioned in the text under their non-protonated form for clarity.

^{119}Sn Liquid NMR spectroscopy. ^{119}Sn Liquid NMR spectra were recorded at 112 MHz on an AVANCE 300 Bruker spectrometer equipped for double resonance including a BBFO *Z*-gradient Automatic Tune and a Mach probe head. The NMR pulse program is a 1D sequence using a 30-degree flip angle of 3.3 microseconds length. In all the samples, 5 drops of D_2O have been added for locking the magnetic field and for calibration. Spectra were recorded with a 2 s relaxation time and 26 000 scans.

Raman spectroscopy. Micro-Raman measurements were performed using a Horiba Jobin Yvon XPlora equipped with an Olympus microscope. A 40× objective with a long working distance has been used. The focus point was localized inside the solution, allowing convective mixing which prevents from sample heating. As a consequence, full laser power can be selected, *i.e.*, at the maximum value of 15 mW for a 638 nm laser excitation. The accumulation time was adjusted to a couple of tens of seconds yielding a clear Raman signal.

DFT calculations. Calculations were carried out using the Gaussian 09[30] package at the DFT level by means of the hybrid density functional B3PW91.[31,32] For the Sn,[33] Zn,[34] Ga[35] and Se[33] atoms, the Stuttgart–Dresden pseudopotentials were used in combination with their extended valence basis sets.[33–36] For the sulfur atoms, the augmented and polarized all electron 6-311++G(d,p)[37] basis sets were used. Optimizations were carried out without any symmetry restriction. The nature of the optimized stationary point, minima or transition state has been verified by means of analytical frequency (IR and Raman) calculations at 298.15 K and 1 atm. Compounds have been optimized in water by means of the SMD solvation model implemented in Gaussian 09.[38] Final frequency calculations have also been computed within the SMD implicit solvation scheme.

Solution exchange and infiltration of heterometallic oligomer-capped ultrafine ZnS colloids

Ligand solution-exchange. CZTS nanocrystals were synthesized using a high temperature gas-templated route in molten KSCN. Details of their synthesis and nanocrystal properties are reported in ref. 27. Carbon-containing surface species such as SCN^- identified on the as-synthesized nanocrystals[27] were solution-exchanged using a $(Sn_a–Zn_b–S_c)^{t-}$ oligomer solution initially prepared at $x_{Zn} = 0.33$. In a typical experiment, CZTS nanocrystals prepared as described in ref. 27 were ball-milled in EtOH and later extensively washed with H_2O. After successive centrifugation and redispersion in H_2O, colloidal aqueous dispersions of CZTS nanocrystals were collected and made to come into contact with a $(Sn_a–Zn_b–S_c)^{t-}$, $x_{Zn} = 0.33$, oligomer solution prepared at 0.1 M ([Sn] + [Zn]). After stirring at room temperature for about 16 h, CZTS nanocrystals were recovered by using an ultracentrifuge at 16 000 rpm and redispersed into a fresh aliquot of the $(Sn_a–Zn_b–S_c)^{t-}$, $x_{Zn} = 0.33$, oligomer solution. This operation was repeated three times. The solid nanocrystals were finally redispersed into 0.01 M $(NH_4)_2S$ yielding a nanocrystal ink of ~35 g L^{-1}.

Infiltration of oligomer capped-ZnS colloids into CZTS nanocrystal films. A purified oligomer capped-ZnS colloid dispersion ($x_{Zn} = 0.66$) was prepared using a similar procedure to that previously described for the $x_{Zn} = 0.33$ oligomer solution. A 2.2 μm thick CZTS nanocrystal film was first prepared by the multi-coating deposition technique onto a glass/Mo electrode. Using a diluted oligomer capped-ZnS colloid dispersion (0.02 M Zn + Sn), infiltration was performed by successive dip coatings (v = 50 mm min^{-1}) onto freshly prepared CZTS nanocrystal films.

Solar cell fabrication

Crack-free Cu_2ZnSnS_4 films were prepared by dip coating the glass/Mo electrode into a $(Sn_a–Zn_b–S_c)^{t-}$ oligomer-capped CZTS nanocrystal aqueous dispersion. Typical conditions for dip coating were v = 200 mm min^{-1}. Crack-free films exhibiting a final thickness of about 2.2 μm were achieved after multiple depositions (18 layers) from aqueous Cu_2ZnSnS_4 dispersions (c = 35 g L^{-1}) under air atmosphere. Complete carbon purification of nanocrystal films was achieved by implementing a purification step (500 °C 30 min, 125 mg Se) in our annealing process. Densification of the CZTS films was performed under selenium partial pressure (125 mg Se) at 580 °C. The surface of the solar cells was S = 2 × 2 mm^2.

Results and discussion

Monometallic M^{n+} (M^{n+} = Sn(IV), Ga(III) or Zn(II)) chalcogenide oligomers

Water-soluble monometallic chalcogenide oligomer formation domains (Fig. S1a and S1b†) were determined on reaction mixtures prepared at [M] = 0.1 M, (M = Sn(IV), Ga(III) or Zn(II)). These formation domains were explored using the two key parameters s and h (or oh), s = $[S^{2-}]/[M]$, h = $[H^+]/[M]$, oh = $[OH^-]/[M]$.

Sn(IV)–S(II) system. Limpid, green-yellow $(Sn_aS_b)^{t-}$ solutions were achieved in a large domain of s and h (or oh) values, $4 \le s \le 12$ and $0 \le h \le 1.75$, $0 \le$ oh ≤ 9.5, with the pH ranging from 8.9 to 10.7. Under high pH conditions, previous studies[16,17] describing the synthesis of chalcogenide complexes formed from solid metallic sulfide dissolution report the formation of a unique $(Sn_2S_6)^{4-}$ chalcogenide complex. For our sample prepared under highly basic conditions, oh = $[OH^-]/[Sn^{4+}]$ = 9.5 (Fig. S2†), Electrospray Ionization Mass Spectrometry (ESI-MS) data reveal a distribution of short oligomers including $(SnS_3)^{2-}$, $(Sn_2S_5)^{2-}$, and $(Sn_3S_7)^{2-}$. Interestingly, while $(SnS_3)^{2-}$, $(Sn_2S_6)^{4-}$, and $(Sn_3S_7)^{2-}$ oligomers were also identified in the solutions prepared at lower pH, $0 \le h \le 1.75$, an intense signal arising from the $(Sn_4S_{10})^{4-}$ oligomer was detected (Fig. 1a and S3a†). For these monometallic $(Sn_a–S_b)^{t-}$ solutions prepared at slightly basic pH, the liquid ^{119}Sn NMR spectrum shows peaks at δ = 55 ppm and δ = 77 ppm. The peak at δ = 55 ppm was previously assigned to $(Sn_2S_6)^{4-}$ species while the peak at δ = 77 ppm was attributed to mononuclear complexes such as $(SnS_4)^{4-}$or $(SnS_3)^{2-}$.[16] Although the presence of the $(Sn_4S_{10})^{4-}$ oligomer was clearly demonstrated by ESI-MS, the peak at −60 ppm previously tentatively attributed[16] to these polymerized species $(Sn_4S_{10})^{4-}$ was not observed in our spectrum. Note that the Raman spectrum recorded on this slightly basic solution reveals a main broad peak centered at 345 cm^{-1} and a secondary peak at 370 cm^{-1}.

The structures of these $(Sn_a–S_b)^{t-}$ oligomers were previously reported in the literature.[14] Previous data have demonstrated that the $(Sn_4S_{10})^{4-}$ oligomers display an adamantane scaffold.[14] Concerning these $(Sn_4S_{10})^{4-}$ oligomers, the relative stability of a linear polytetrahedron structure with respect to the adamantane-like one has been assessed by DFT calculations. Consistent with the experimental data previously reported,[14] our calculations indicate that the adamantane $\mathbf{T_2}$ structure is more stable than the linear polytetrahedron $(\mathbf{T_1})_4$ by 11.8 kcal mol^{-1} ($\Delta_rG°$ value).

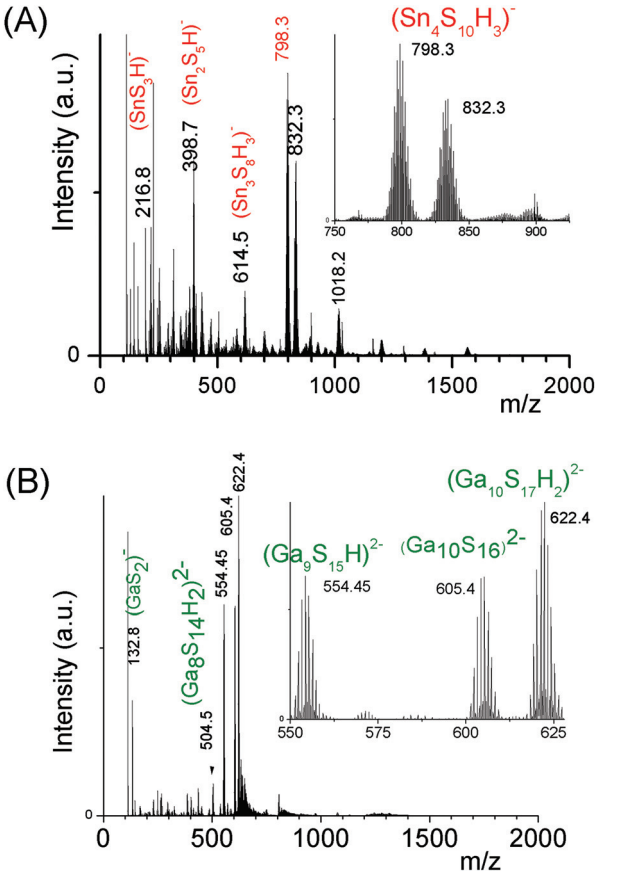

Fig. 1 Negative ion ESI MS spectra of monometallic oligomers. (A) $(Sn_aS_b)^t$ oligomers prepared from a Sn^{4+} solution ($[H^+]/[Sn^{4+}]$ = 1.5), Sn(IV) = 0.1 M and s = 4. Insert: Zoom showing the presence of tetra mers. (B) $(Ga_aS_b)^t$ oligomer solution, pH 8.9, showing the presence of doubly charged oligomers. The oligomer solution is synthesized from a Ga^{3+} solution ($[H]/[Ga^{3+}]$ = 0), at Ga(III) = 0.1 M and s = 6. This solution is prepared by re dispersion of the solid in 0.01 M $(NH_4)_2S$. Insert: Zoom showing the presence of $(Ga_aS_b)^t$ oligomers including up to 10 Ga(III) cations.

Ga(III)–S system. While soluble oligomers were synthesized in the Sn(IV)–S(II) system over the whole range of $[OH^-]/[Sn^{4+}]$ ratios investigated, limpid dispersions of oligomers in the Ga(III)–S(II) system ($[Ga^{3+}]$ = 0.1 M) were achieved only in highly basic reaction mixtures ($6 \le [OH^-]/[Ga^{3+}] \le 10$). Under less basic conditions, $[OH^-]/[Ga^{3+}] \le 6$ and $[H^+]/[Ga^{3+}] \le 1$, limpid oligomer solutions were exclusively observed after $(NH_4)_2S$ and NH_4Cl by-product removal from the solutions (Fig. S1b†). Similarly to the Sn(IV)–S(II) system, electrospray ionization mass spectrometry data indicate the formation of oligomers displaying various polycondensation degrees depending on the synthesis pH conditions. Under highly basic conditions, a high proportion of short, low molecular mass $(GaS_2)^-$

oligomers was identified, consistently with the lower sensitivity to the ionic strength of these oligomer solutions. When synthesized in the lowest pH range, the ESI-MS spectrum (Fig. 1b) reveals a large distribution of oligomers including $(GaS_2)^-$, $(Ga_8S_{14})^{4-}$, $(Ga_9S_{14})^-$, $(Ga_9S_{15})^{3-}$, and $(Ga_{10}S_{17})^{4-}$. Interestingly, predominant peaks corresponding to large $(Ga_8S_{14})^{4-}$, $(Ga_8S_{14})^{4-}$, $(Ga_9S_{14})^-$, $(Ga_9S_{15})^{3-}$, and $(Ga_{10}S_{17})^{4-}$ oligomers containing up to 10 Ga atoms were identified in a small window of pH values, pH < 8.5. Note that under these pH conditions, the tetrameric $(Ga_4S_{10})^{4-}$ oligomer was not detected in the solutions. The high molecular mass of the identified oligomers is consistent with their low solubility or their high sensitivity to the ionic strength observed for these oligomers. Consistently, size determination by dynamic light scattering (DLS) reveals a large hydrodynamic size, 30 nm < d_{50} < 40 nm, for dispersions prepared at $[H^+]/[Ga^{3+}]$ = 1.5 while dispersions prepared at $[OH^-]/[Ga^{3+}]$ = 7 displayed a hydrodynamic size of 3 nm. Concerning the oligomer dispersions synthesized under less basic conditions, the large discrepancy observed between the high value of d_{50} and the low number of metal centers of the oligomer suggests the presence of aggregated entities. As revealed by ESI-MS and DLS characterization, more polymerized species are thus formed in the Ga(III)–S(II) system compared to the Sn(IV)–S(II) system. Indeed, the lower charge of Ga(III) compared with Sn(IV) makes it possible to form the tricoordinate sulfur sites needed for the formation of **T₃** clusters, $(Ga_{10}S_{20})^{10-}$, containing up to 10 Ga atoms.[39] In addition, the large variety of polymerized oligomers identified by ESI-MS, namely $(Ga_9S_{15})^{3-}$, $(Ga_{10}S_{17})^{4-}$, $(Ga_{10}S_{16})^{2-}$ and $(Ga_{10}S_{17})^{4-}$, are likely built adopting the **T₃** framework. Indeed, the large sulfide anion deficiency observed in these oligomers suggests the formation of compact rather than linear structures.

Zn(II)–S(II) system. Consistent with previous reports describing the very low aqueous solubility of ZnS,[40] no soluble oligomer dispersion was achieved in the Zn(II)–S(II) system using our mild process route in spite of the large range of $[S^{2-}]/[Zn^{2+}]$ and $[OH^-]/[Zn^{2+}]$ ratios investigated. This result is consistent with the higher degree and the faster kinetics of metal chalcogenide condensation gradually observed from tetravalent to bivalent metal cations. Indeed, the better control of condensation kinetics observed on the high-valent metal cation arises from the higher number of S^{2-} anions required to satisfy the local charge density matching.

Heterometallic Sn(IV)–Zn(II) chalcogenide oligomers

Sn(IV)–Zn(II)–S(II) system. Key parameters describing the formation conditions of $(Sn_a–Zn_b–S_c)^{t-}$ oligomers were $s = [S^{2-}]/([Sn^{4+}] + [Zn^{2+}])$ and $h = [H^+]/[Sn^{4+}] + [Zn^{2+}]$. Fig. S1c† depicts the results obtained for ([Zn] + [Sn]) = 0.1 M and x_{Zn} = 0.33, where $x_{Zn} = [Zn]/([Zn] + [Sn])$. Compared with the pure Sn(IV)–S oligomer formation domain, a smaller range of, limpid to the naked eye, heterometallic $(Sn_a–Zn_b–S_c)^{t-}$ oligomer dispersions was observed in the range of $3 \le s \le 5$, $h \le 1$ and $0 \le oh \le 6.0$ with the corresponding pH values varying from 8.6 to 11.6. The formation diagram of soluble oligomer dispersions synthesized by the addition of a (Zn^{2+}, Sn^{4+}) solution onto the $(NH_4)_2S$ solution was determined for various x_{Zn} values, $0.20 \le x_{Zn} \le 0.85$ (Fig. 2). Limpid dispersions to the naked eye were observed in a large range of x_{Zn}, $0.0 \le x_{Zn} \le 0.75$. Consistently, more highly concentrated limpid solutions were achieved at compositions close to the highest soluble $(Sn_a–S_b)^{t-}$ oligomer.

An ESI-MS investigation performed on these limpid solutions (Fig. 3a) without any dilution synthesized at different x_{Zn} values, x_{Zn} = 0.33, 0.50, and 0.66, revealed the presence of oligomers displaying similar compositions but in different proportions as shown by the relative intensities of the ESI-MS peaks. In these solutions, monometallic Sn chalcogenide oligomers including $(SnS_3)^{2-}$, $(Sn_2S_5)^{2-}$, $(Sn_3S_7)^{2-}$, $(Sn_3S_8)^{4-}$, and $(Sn_4S_{10})^{4-}$ were detected in association with heterometallic oligomers (Fig. 3b). Indeed, mass spectrometry data clearly reveal the presence of heterometallic oligomers including $(SnZnS_4)^{2-}$, $(Sn_{2.0}Zn_{1.0}S_6)^{2-}$, $(Sn_{2.0}Zn_{1.0}S_7)^{4-}$, $(Sn_{3.0}Zn_{1.0}S_9)^{4-}$, and $(Sn_{3.0}Zn_{1.0}S_8)^{2-}$ with a larger proportion of the four metal center oligomers.

Interestingly, as shown by the isotope patterns reported in Fig. S3c,† two different heterometallic oligomers characterized by a different number of sulfide anions and possessing four metal centers including a sole Zn cation, $(Sn_{3.0}\ Zn_{1.0}\ S_8)^{2-}$ and $(Sn_{3.0}\ Zn_{1.0}\ S_9)^{4-}$, were clearly identified. From quasi-elastic light scattering investigation, a hydrodynamic average size of 2 nm, consistent with the oligomer low molecular mass, was determined on samples prepared at $x_{Zn} \le 0.33$. An increase of x_{Zn} results in larger mean hydrodynamic diameter values

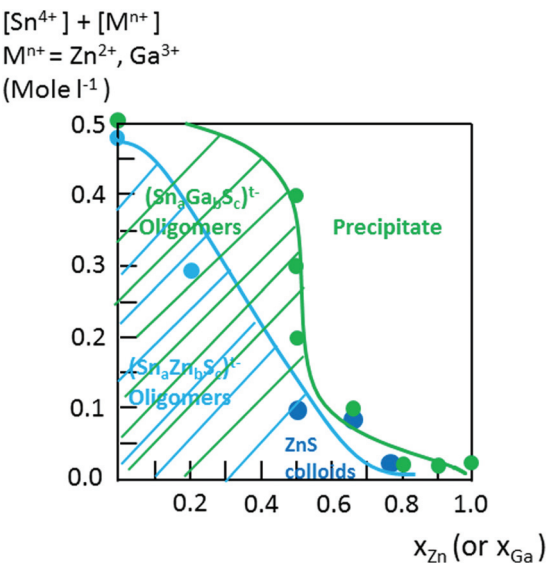

Fig. 2 Oligomer formation diagrams, $([Sn^{4+}] + [M^{n+}])$ = 0.1 M, M = Zn^{2+} or Ga^{3+}. The hatched blue area represents the soluble $(Sn_a\ Zn_b\ S_c)^t$ oligomers domain synthesized by the addition of (Zn^{2+}, Sn^{4+}) solution $(H^+/(Zn + Sn) = 0.5)$ onto a $(NH_4)_2S$ solution at s = 6. Dark blue circles represent the formation of ZnS colloid dispersions. The hatched green area represents the domain of $(Sn_a\ Ga_b\ S_c)^t$ soluble oligomers prepared from (Ga^{3+}, Sn^{4+}) solutions, $([H^+]/[Sn] + [Ga] = 0)$ and S^{2-} solutions at s = 6.

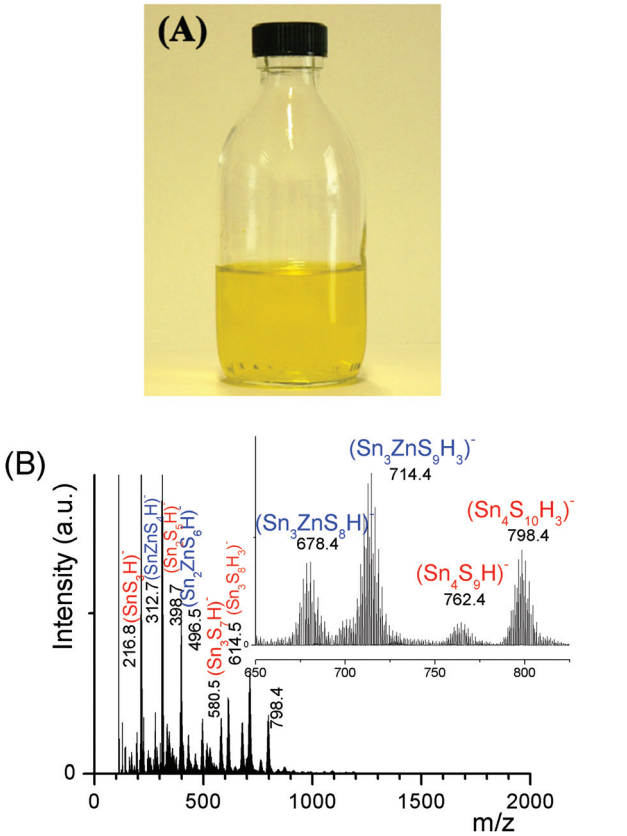

Fig. 3 (A) Photograph of a $(Sn_a\ Zn_b\ S_c)^t$ oligomer solution. (B) Negative ion ESI MS spectrum of $(Sn_a\ Zn_b\ S_c)^t$ oligomer solutions prepared from $(Sn^{4+} + Zn^{2+})$ solutions, $([H^+]/([Sn^{4+}] + [Zn^{2+}]) = 1.5)$, $[S^{2-}]/([Sn^{4+}] + [Zn^{2+}]) = 6$ and $([Sn] + [Zn]) = 0.1$ M. $x_{Zn} = 0.33$. Insert: Zoom showing the presence of heterometallic tetramers.

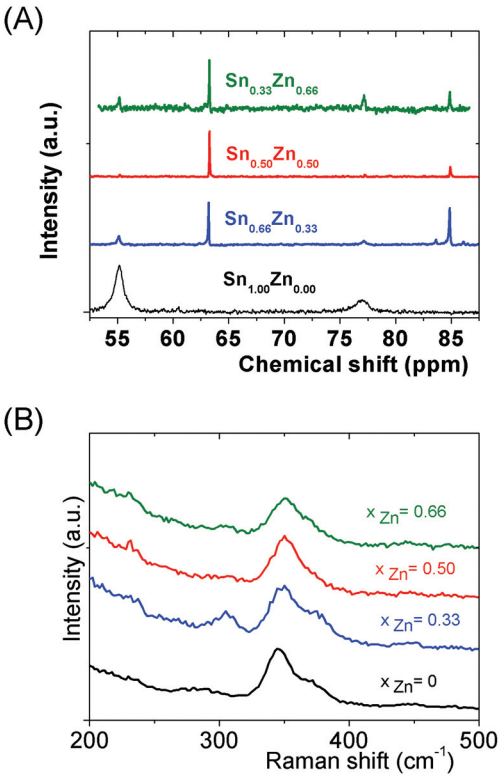

Fig. 4 $(Sn_a\ Zn_b\ S_c)^t$ oligomer solutions prepared from $(Sn^{4+} + Zn^{2+})$ solutions, $([H^+]/([Sn^{4+}] + [Zn^{2+}]) = 1.5)$, $[S^{2-}]/([Sn^{4+}] + [Zn^{2+}]) = 6$ and $([Sn] + [Zn]) = 0.1$ M. (A) ^{119}Sn Liquid NMR spectra recorded on $(Sn_a\ Zn_b\ S_c)^t$ oligomer dispersions synthesized at various x_{Zn} values, $x_{Zn} = 0.00$, 0.33, 0.50 and 0.66. (B) Raman spectra recorded on dispersions prepared at $x_{Zn} = 0.00$, 0.33, 0.50 and 0.66.

(Fig. S4†). Indeed, dispersions prepared at x_{Zn}, $0.33 \leq x_{Zn} \leq 0.50$, show a mean size of 5 nm while dispersions synthesized at $x_{Zn} = 0.66$ possess a hydrodynamic diameter of around 18.5 nm. Although all these dispersions are limpid to the naked eye, these data suggest that the $(Sn_a–Zn_b–S_c)^{t-}$ heterometallic oligomers are mainly obtained at low x_{Zn} values, $x_{Zn} \leq 0.33$, while dispersions formed for $x_{Zn} > 0.40$ probably contain predominantly ZnS colloids. Interestingly, the size monodispersity of the nano-objects observed at $x_{Zn} = 0.5$ shows the formation of a monodisperse population of ZnS colloids stabilized by $(Sn_{4-x}Zn_xS_z)^{t-}$ oligomers. Liquid ^{119}Sn NMR spectra recorded on the various dispersions show traces at $\delta =$ 55 ppm and $\delta = 77$ ppm previously observed on the monometallic $(Sn_aS_b)^{t-}$ oligomers and respectively attributed to $(Sn_2S_6)^{4-}$ and SnS_4^{4-}/SnS_3^{2-} species.[16] More importantly, additional peaks of higher intensities are clearly observed at $\delta = 63$ ppm and $\delta \sim 82/85$ ppm for the entire range of x_{Zn} investigated (Fig. 4a). Because a unique heterometallic tetramer oligomer possessing a lonely Zn cation was observed whatever the x_{Zn} value, liquid ^{119}Sn NMR spectra recorded on the various dispersions display identical additional peaks. In addition, the larger intensity of these additional peaks observed on the $x_{Zn} = 0.33$ dispersion is consistent with the largest heterometallic oligomer proportion in this dispersion. Therefore, the experimental chemical shifts observed at $\delta = 63$ ppm and $\delta \sim 82/85$ ppm result from the incorporation of the Zn cation into the four metal center $(Sn_{3.0}Zn_{1.0}S_z)^{t-}$ oligomers. Raman spectra recorded on the various dispersions exhibit a main broad peak centered at 345 cm^{-1} and a secondary peak at 370 cm^{-1} (Fig. 4b). Although deconvolution of the main broad peak shows a slight increase of the frequency of this peak observed with increased x_{Zn} (Fig. 4b), full assignment of these peaks remains inconclusive due to the overlapping of the different peaks in this region. Indeed, $\nu_1(A_1)$ and $\nu_3(T_2)$ Raman frequencies[13] of SnS_4^{4-} were reported respectively at 348 and 344 cm^{-1} while the Raman frequencies of 1-longitudinal-optical phonon mode of cubic ZnS[41] and quasi longitudinal mode of Wurtzite ZnS[42] were respectively reported to be 343 cm^{-1} and 350 cm^{-1}.

Sn(IV)–Zn(II)–Se(II) system. The versatility of our mild process route was demonstrated by the formation of heterometallic oligomers in the Zn(II)–Sn(II)–Se(II) system. In a first stage, a procedure for the formation of $(NH_4)_2Se$ solution was developed. Se^{2-} solutions were obtained from the dissolution of the Se metal into NH_3 solutions using Na^+ SO_2CH_2OH (Na hydroxyl-methane-sulfinate or Rongalite) as a reducing agent. Note that the $(NH_4)_2Se$ solution synthesis was

conducted under N_2 to avoid the Se^{2-} oxidation by air. As for the sulfide oligomer heterometallic synthesis, $(Sn_a–Zn_b–Se_c)^{t-}$ oligomers were prepared by instantaneous addition of a Sn^{4+} (or Sn^{4+}, Zn^{2+}) chloride solution to the as-synthesized $(NH_4)_2Se$ solution. Fine-tuning of the final pH of the oligomer solutions, in particular in the slightly basic pH range, was achieved through a pre-adjustment of the acidity (h = $[H^+]/([Sn^{4+}] + [Zn^{2+}])$) of the Sn^{4+} (or Sn^{4+} + Zn^{2+}) chloride solution or the basicity of the $(NH_4)_2Se$ solution.

The mass spectrum of the $(Sn_aSe_b)^{t-}$ monometallic oligomer solution prepared at $[H^+]/[Sn] = 0.5$, $s = 3$, $[Sn] = 0.1$ displays predominant peaks recorded at m/z = 634.4 and 1267.80 (Fig. 5a), which are respectively assigned to $(Sn_2Se_5)^{2-}$ and $(Sn_4Se_{10})^{4-}$ species. Similarly to the $(Sn_aS_b)^{t-}$ oligomer solution, we thus clearly demonstrate the presence of $(Sn_4Se_{10})^{4-}$ oligomers in slightly basic solutions. Similarly to the Sn–Zn–S system, investigation of the Sn–Zn–Se system at various x_{Zn} values, x_{Zn} = 0.33, 0.5 and 0.66, reveals the formation of heterometallic oligomers displaying similar compositions, independently of x_{Zn}. Simultaneously with the presence of $(SnSe_3)^{2-}$, $(Sn_2Se_5)^{2-}$, and $(Sn_4Se_{10})^{4-}$ homometallic oligomers, $(SnZnSe_4)^{2-}$, $(Sn_3ZnSe_8)^{2-}$, and $(Sn_3ZnSe_9)^{4-}$ heterometallic oligomers were identified by ESI-MS in the solutions prepared at various x_{Zn} values, x_{Zn} = 0.33 (Fig. 5b), 0.50 and 0.66. As illustrated by the isotope patterns, various heterometallic oligomers containing one Zn cation and different numbers of sulfide anions $(Sn_{1.0}Zn_{1.0}Se_{4.0})^{2-}$, $(Sn_{3.0}Zn_{1.0}Se_{8.0})^{2-}$, and $(Sn_{3.0}Zn_{1.0}Se_{9.0})^{4-}$ were clearly observed (Fig. 5 and S3c†). Nevertheless, in contrast to the tetramers, no stable structure was achieved from our DFT calculations for the $(Sn_{1.0}Zn_{1.0}Se_4)^{2-}$ oligomer. Therefore, the $(Sn_{1.0}Zn_{1.0}Se_4)^{2-}$ oligomer experimentally observed by mass spectrometry probably arises from fragmentation in the mass spectrometer. Raman spectra of $(Sn_a–Zn_b–Se_c)^{t-}$ oligomers were recorded on the solution prepared at x_{Zn} = 0.33. Peaks were observed at 208 cm^{-1}, 194 cm^{-1}, 173 cm^{-1} and 162 cm^{-1} (Fig. 5c). Note that the adamantane structure of the monometallic tetramer $(Sn_4Se_{10})^{4-}$ was previously and unambiguously determined.[14] In addition, experimental Raman peaks recorded on the monometallic $(Sn_aSe_c)^{t-}$ oligomer observed in the region of 199 cm^{-1} (ν_1·A_1) were previously assigned[43] to low molecular species such as the $(SnSe_4)^{4-}$ monomer while peaks observed in the region of 178 cm^{-1} (ν_2·A_1) were assigned to adamantane-like tetrameric species.[43] In contrast to SnS_4^{4-} and ZnS vibrations, no significant overlapping exists concerning the Raman peaks of the $(Sn_3Zn_{1.0}Se_9)^{4-}$ heterometallic selenide oligomer. In order to better clarify the structure of the latter heterometallic tetramer, Raman spectra of these oligomers were computed at a DFT level on these selenide oligomers. We report the calculated Raman shifts and scattering activities of $(Sn_aSe_c)^{t-}$ and $(Sn_a–Zn_b–Se_c)^{t-}$ oligomers in Table 1.

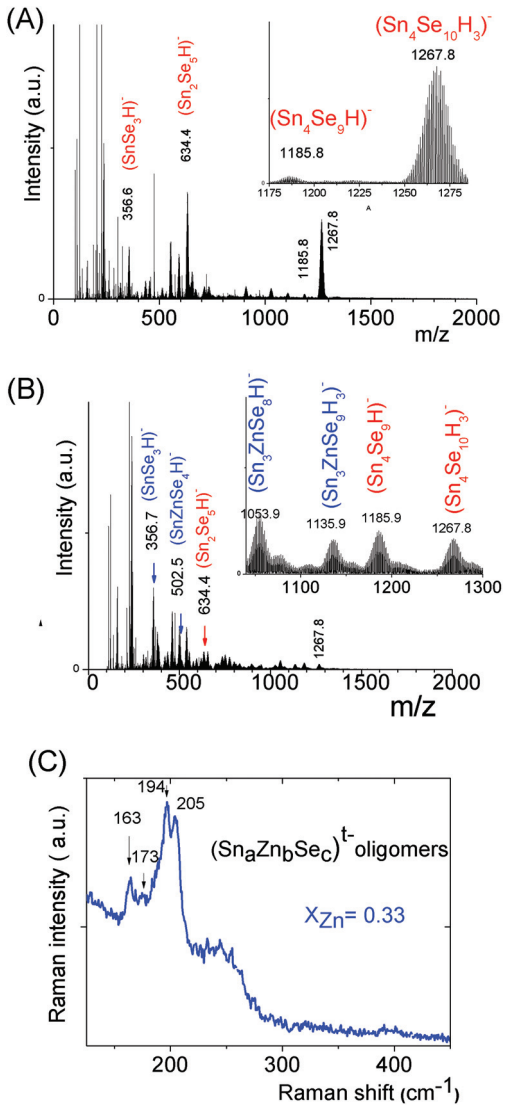

Fig. 5 $(Sn_a\ Se_c)^t$ and $(Sn_a\ Zn_b\ Se_c)^t$ oligomer solutions prepared from (Sn^{4+} + Zn^{2+}) solutions, ($[H^+]/([Sn^{4+}] + [Zn^{2+}]) = 0.5$), $[Se^2]/([Sn^{4+}] + [Zn^{2+}]) = 3$ and ([Sn] + [Zn]) = 0.1 M. (A) Negative ion ESI MS spectrum of a $(Sn_a\ Se_c)^t$ solution. (B) Negative ion ESI MS spectrum of $(Sn_a\ Zn_b\ Se_c)^t$ oligomer solutions prepared at x_{Zn} = 0.33. (C) Raman spectrum of the $(Sn_a\ Zn_b\ Se_c)^t$ oligomer solution, x_{Zn} = 0.33.

From our calculated Raman shifts, some assignments of the various experimental Raman peaks recorded on the $(Sn_aZn_bSe_c)^{t-}$ oligomer solutions could be made:

- Main vibrations of low molecular mass species were determined from our calculations in the 205 cm^{-1}–215 cm^{-1} frequency region: $(SnSe_3)^{2-}$ at 208 cm^{-1} and $(Sn_2Se_5)^{2-}$ at 212 cm^{-1}. Experimental peaks respectively observed at 194 cm^{-1} and 205 cm^{-1} were thus respectively assigned to $(SnSe_3)^{2-}$ and $(Sn_2Se_5)^{2-}$ species, clearly identified on the ESI-MS spectra.

- Vibrations associated with the linear $(Sn_4Se_{10})^{4-}$ structure were determined from our DFT calculations at 201 cm^{-1} while the main vibration of the $(Sn_4Se_{10})^{4-}$ tetramer adamantane-like structure was determined in the region 170–180 cm^{-1}, corroborating the data previously reported in the literature.[43] From these observations, experimental peaks observed in the region 160–180 cm^{-1} clearly suggest the formation of tetrameric heterometallic oligomers displaying an adamantane-like

Table 1 Calculated Raman shifts and scattering activities of $(Sn_aSe_b)^t$ and $(Sn_aZn_bSe_c)^t$ oligomers. The frequency of the main peak has been determined by convoluting Lorentzian functions whose amplitudes are proportional to computed Raman activity intensities and a half band width of 20 cm ^{1}

Monomers Oligomers	Frequency, cm^{-1} (Raman scattering activity >20 $Å^4$ amu^{-1})
$(SnSe_3)^{2-}$	**208**(294), 264(34), 264(35) Main peak: **208**
$(SnSe_4)^{4-}$	**184**(318), 210(44), 211(44), 212(44)
$(Sn_2Se_5)^{2-}$	49.3(21), 58.6(24), 102.1(39), **165.0**(81), **211.5**(346), **223.3**(74), 263.2(32), 297.7(38) Main peak: **212**
$(Sn_4Se_{10})^{4-}$ linear	**201**, 256
ada $(Sn_4Se_{10})^{4-}$	43.6(20), 68.4(50), 68.8(50), 69.0(54), **101.5**(211), **173.5**(589), 220.5(43), 221.0(43), 221.2(43), 247.0(50), **247.2**(53), **248.3**(50), **253.3**(189) Main peak: **173**
$(SnZnSe_4)^{2-}$	Not stable molecular structure; dissociative
ada $(Sn_3ZnSe_9)^{4-}$	73.2(27), 74.8(26), 77.7(46), 95.1(44), 118.5(62), **173.1**(499), 208.6(40), 209.6(44), 221.8(25), **227.4**(148), 245.3(41), 246.6(39), 247.5(89) Main peak: **173**

structure. Although our DFT calculations show that the incorporation of one Zn cation into the adamantane-like tetrameric structure does not result in a significant variation of the main Raman peak frequency, we tentatively assign the peaks experimentally observed at 173 and 162 cm^{-1} to the non-substituted $(Sn_4Se_{10})^{4-}$ and Zn-substituted $(Sn_3ZnSe_9)^{4-}$ adamantane-like oligomers. The adamantane-like structures of the $(Sn_3ZnSe_8)^{2-}$ and $(Sn_3ZnSe_9)^{4-}$ oligomers as optimized by DFT calculations are reported in Fig. 6.

Heterometallic Sn(IV)–Ga(III) chalcogenide oligomers

In contrast to the formation of $(Sn_a–Zn_b–S_c)^{t-}$ oligomers, soluble $(Sn_a–Ga_b–S_c)^{t-}$ oligomer solutions were achieved in the whole range of x_{Ga} yielding a larger oligomer formation domain (Fig. 2). Similarly to the Sn(IV)–Zn(II)–S(II) system, more highly concentrated $(Sn_a–Ga_b–S_c)^{t-}$ oligomer solutions were observed for compositions close to the most soluble $(Sn_aS_c)^{t-}$ oligomer. Indeed, oligomer solutions with concentrations up to ([Sn] + [Ga]) > 0.4 M were prepared in the presence of NH_4Cl by-products for x_{Ga} values up to x_{Ga} = 0.5 while oligomer solutions prepared at higher x_{Ga} values exhibit a much lower ([Sn] + [Ga]) concentration.

An ESI-MS investigation performed on various $(Sn_a–Ga_b–S_c)^{t-}$ oligomer solutions, $0.33 \leq x_{Ga} \leq 0.80$, clearly indicates that these solutions contain oligomer distributions (Fig. 7). Interestingly, the composition and concentration of these oligomers depend on the x_{Ga} molar fraction of the oligomer dispersion. In contrast to the $(Sn_a–Zn_b–S_c)^{t-}$ oligomer solutions, a very low proportion of monometallic oligomers containing exclusively Ga(III) cations, *i.e.* $(GaS_2)^-$, $(Ga_2S_4)^{2-}$ or Sn(IV) cations $(Sn_4S_{10})^{4-}$, was determined from the relative intensities of the ESI-MS peaks. More importantly, a larger proportion of heterometallic oligomers including $(Ga_3SnS_8)^{3-}$, $(Ga_2Sn_2S_8)^{2-}$, $(Ga_2Sn_2S_9)^{4-}$, $(Ga_2Sn_2S_{10})^{6-}$, and $(GaSn_3S_{10})^{5-}$ was detected by ESI-MS in these solutions (Fig. 7 and S3d†). It is worth mentioning that these $(Ga_aSn_bS_c)^{t-}$ heterometallic oligomers are less polymerized compared to the monometallic $(Ga_aS_c)^{t-}$ oligomers synthesized under similar conditions. Indeed, these heterometallic oligomers are shown to be mainly composed of four metal centers incorporating up to three Ga(III) cations.

We can note that the large variety of heterometallic tetrameric oligomers $(Ga_3SnS_8)^{3-}$, $(Sn_3GaS_{10})^{5-}$, and $(Sn_2Ga_2S_{10})^{6-}$ possessing various Ga(III) cation and sulfide anion contents display various charges, thus allowing charge control by a fine tuning of the x_{Ga} value. Liquid ^{119}Sn NMR spectra recorded on the $(Sn_a–Ga_b–S_c)^{t-}$ oligomer solutions display similar features to those observed on $(Sn_a–Zn_b–S_c)^{t-}$ oligomer solutions. Peaks at δ = 55 ppm and δ = 77 ppm and respectively assigned to the monometallic $(Sn_2S_6)^{4-}$ and SnS_4^{4-}/SnS_3^{2-} species were observed on the sample synthesized at x_{Ga} = 0.33. Consistently, a significant decrease of the intensity of these peaks is observed with increased number of Ga(III) atoms in the heterometallic tetramers. More interestingly, as for $(Sn_a–Zn_b–S_c)^{t-}$ oligomer solutions, numerous additional peaks which were not observed on monometallic $(Sn_a–S_c)^{t-}$ oligomers were clearly detected at δ = 82/85 ppm on heterometallic $(Sn_a–Ga_b–S_c)^{t-}$ oligomer solutions (Fig. 8a). Compared with the spectra recorded on $(Sn_a–Zn_b–S_c)^{t-}$ oligomer solutions, the larger

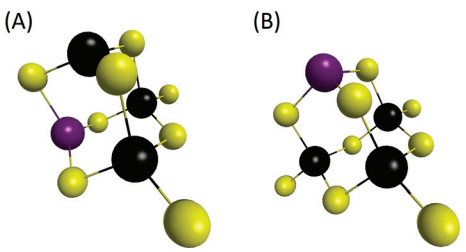

Fig. 6 Oligomer computed structures determined by DFT calculations. Yellow: Se, black: Sn, violet: Zn. (A) $(Sn_3ZnSe_8)^2$. (B) $(Sn_3ZnSe_9)^4$.

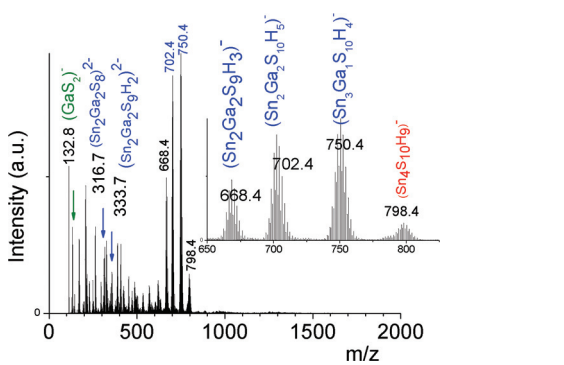

Fig. 7 Negative ion ESI MS spectrum of $(Sn_a\ Ga_b\ S_c)^t$ oligomer solutions prepared from $(Sn^{4+} + Ga^{3+})$ solutions, $([H^+]/([Sn^{4+}] + [Ga^{3+}]) = 0)$ at x_{Ga} = 0.5, $[S^2]/([Sn^{4+}] + [Ga^{3+}]) = 6$ and ([Sn] + [Ga]) = 0.1 M showing the presence of heterometallic tetrameric oligomers.

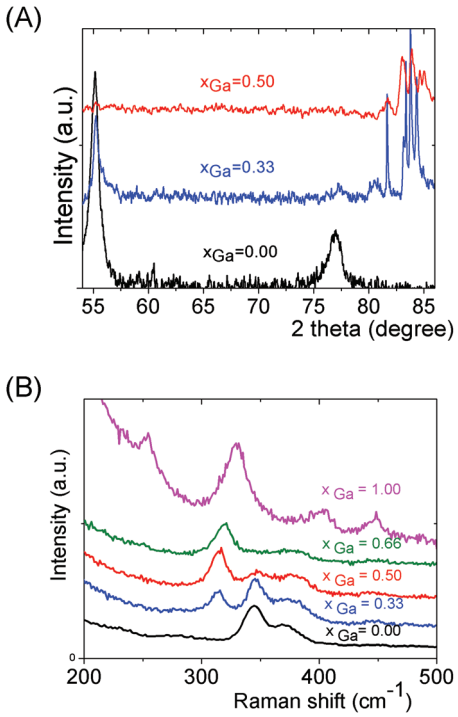

Fig. 8 $(Sn_a\ Ga_b\ S_c)^t$ oligomer solutions at various x_{Ga} values prepared by the addition of a $(Sn^{4+} + Ga^{3+})$ solution $([H^+]/([Sn^{4+}] + [Ga^{3+}]) = 0)$ into a $(NH_4)_2S$ solution at $[S^{2\ }]/([Sn^{4+}] + [Ga^{3\ }] +]) = 6$ and $([Sn] + [Ga]) = 0.1$ M. (A) ^{119} Sn liquid NMR spectra. (B) Raman spectra. Spectra of $(Sn_a\ S_c)^t$ and $(Ga_b\ S_c)^t$ monometallic oligomer solutions are also reported.

number of peaks appearing in the chemical shift range 82/85 ppm highlights the higher number of Sn environments observed in $(Sn_a–Ga_b–S_c)^{t-}$ oligomers. Fig. 8b shows Raman spectra recorded on various $(Sn_a–Ga_b–S_c)^{t-}$ oligomer solutions (x_{Ga} = 0.00, 0.33, 0.5, 0.66 and 1.00) prepared under slightly basic conditions. Fine inspection of these spectra suggests a solid solution behavior involving two non-interacting vibration modes. Although the Raman behavior of solid solution is quite complicated, polar modes usually transfer their intensities[44] while both the position and intensities of transverse and longitudinal modes in solid solution are linked.[45] Fig. 8b shows a continuous variation of both the Raman intensity and the Raman shifts of the Ga–S vibration (310–320 cm^{-1}) and of the Sn–S vibration (345 cm^{-1}) observed for the whole range of solid solutions. $Ge_4S_{10}{}^{4-}$, $Ge_4Se_{10}{}^{4-}$, $Sn_4S_{10}{}^{4-}$, and $Sn_4Se_{10}{}^{4-}$ adamantane-like structures were previously reported as the predominant condensation structures in monometallic oligomer solutions of lower pH values.[14] To determine the structure of the heterometallic chalcogenide tetramers in the Sn(IV)–Ga(II)–S(II) system, Raman spectra of $(Sn_{4-x}Ga_xS_{10})^{4-}$ adamantane-like species were thus computed at a DFT level. Table S5† reports the calculated Raman frequency of the main peak for various species, $0 \leq x_{Ga} \leq 1$. The frequency of the main peak has been determined by convoluting Lorentzian functions whose amplitudes are proportional to computed Raman activity intensities and a half-band width of 20 cm^{-1}. Although the main peak values are overestimated, these calculations clearly show a lower frequency of the main peak for the $(Ga_4S_{10})^{4-}$ adamantane tetramer compared with the $(Sn_4S_{10})^{4-}$ tetramer. Thus, experimentally determined Raman shifts on the $(Ga_4S_{10})^{4-}$ and $(Sn_4S_{10})^{4-}$ adamantane tetramer solutions are consistent with the DFT results. Although more data including dynamic effective charge and intensity transfer between polar modes are needed to propose a more complete model, the continuous variation of the Raman shifts experimentally observed in the whole range of solid solutions demonstrates that the various $(Sn_a–Ga_b–S_c)^{t-}$ heterometallic oligomers preserve the adamantane structure. The structures of the $(Sn_3GaS_{10})^{5-}$ $(Sn_2Ga_2S_{10})^{6-}$ and $(Sn_2Ga_2S_9)^{4-}$ oligomers determined by DFT are reported in Fig. 9.

Heterometallic $(Sn_a–Ga_b–S_c)^{t-}$ oligomers were prepared by our mild process route. Incorporation of a tetravalent cation such as Sn(IV) into the Ga(III) oligomers allows the formation of a series of short, discrete, highly charged tetrameric adamantane oligomers. These heterometallic oligomers were fully characterized by ESI-MS, Raman and ^{119}Sn liquid NMR spectroscopy.

Discussion

Heterometallic chalcogenide oligomer formation results in poly-condensation inhibition. New concepts in synthesis and crystal structure have emerged from recent developments in porous chalcogenides. Incorporation of a lower-valent cation was previously reported to help increase the size of large trivalent metal chalcogenide solid clusters providing the required local charge matching.[39] In contrast, the incorporation of tetravalent cations tends to lower their size. In our experiments, while monometallic Sn(IV)–S and Ga(III)–S oligomers prepared using our mild poly-condensation route were shown to display various oligomer sizes consistent with local charge balance concepts (see the largest $(Ga_{10}S_{17})^{4-}$ soluble monometallic oligomers), the largest soluble discrete heterometallic oligomers achieved by our mild poly-condensation route are mainly short oligomers composed of four metal centers. Thus, by a mild polycondensation process route occurring at room temperature, substitution by a higher-valent metal cation, *e.g.* insertion of Sn(IV) into a Ga(III) chalcogenide framework or of Sn(IV) into a Zn(II) framework, results in poly-condensation inhibition. However, in a control experiment, no

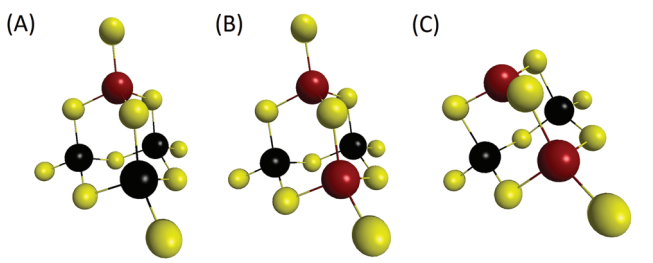

Fig. 9 Computed structures. Yellow: S, black: Sn, red: Ga. (A) $(Sn_3GaS_{10})^5$, (B) $(Sn_2Ga_2S_{10})^6$ and (C) $(Sn_2Ga_2S_9)^4$ oligomers.

soluble heterometallic oligomer was achieved by substitution of Ga(III) into the Zn(II) framework, highlighting the crucial role of the high charge or the high electronegativity of the dopant cation in the chalcogenide polycondensation inhibition.

Control of phase separation. One-pot fabrication of heterometallic oligomers generally involves the use of non-aqueous synthesis methods.[46] We have shown here that chalcogenide poly-condensation from aqueous metallic soluble species can result in heterometallic oligomers. Indeed, heterometallic oligomers are detected by ESI-MS in association with monometallic oligomers, indicating phase separation during the synthetic process. Minimum phase separation yielding a solution possessing mainly heterometallic oligomers was experimentally observed in the III–IV (Ga(III)–Sn(IV)) system compared with the II–IV (Zn(II)–Sn(IV)) system. This highlights the effect of key parameters such as chalcogenide polycondensation kinetics and the local charge balance. Interestingly, a reaction mixture displaying cations in equimolar concentrations ($Sn_{0.5}Ga_{0.5}$ composition) yields a minimal phase separation while producing a variety of heterometallic oligomers.

Control of oligomer charge. These heterometallic chalcogenide oligomers could serve as surface additives for chalcogenide nanocrystal colloidal stabilization or as soluble species for the post-infiltration of porous nanocrystal films. In these applications, synthesis of highly charged oligomers is desirable. A first route to manipulate the charge of heterometallic chalcogenide oligomers is to vary the valence of the substituting cation. Using a divalent cation such as Zn(II), the $(Sn_{3.0}Zn_{1.0}S_8)^{2-}$ oligomer was prepared from $(Sn_{4.0}S_{10})^{4-}$. Higher charged oligomers were achieved with the substitution of Sn(IV) by a trivalent cation ($(GaSn_3S_{10})^{5-}$, $(Sn_2Ga_2S_{10})^{6-}$). Because a variety of oligomers ($(Sn_2Ga_2S_{10})^{6-}$, $(Sn_2Ga_2S_9)^{4-}$, $(Sn_2Ga_2S_8)^{2-}$) were prepared as a result of the lability of the peripheral S^{2-} anion, changing the sulfide concentration might represent another strategy to control oligomer charge.

Heterometallic chalcogenide oligomers as environmentally-friendly building blocks for solar cells

Successful development[1,2] of hydrazine-based metal chalcogenide complexes relies on its easy decomposition to the parent metal chalcogenides without any impurities. Charged, water-soluble, organic-free, heterometallic chalcogenide oligomers involving a residue-free, ammonium cation described here are extremely attractive from an environmental perspective (Fig. S6†). Indeed, the $(Sn_a–Zn_b–S_c)^{t-}$ heterometallic oligomers or $(Sn_a–Zn_b–S_c)^{t-}$-capped ZnS colloids could provide exciting opportunities as building blocks for the design of an all-aqueous process route for low-cost photovoltaic device fabrication. These all-inorganic heterometallic chalcogenide oligomers or ultrafine colloids could serve as dispersants or composition control additives.

Ligand exchange, aqueous colloidal stabilization and Cu_2ZnSnS_4 nanocrystal film formation. The search for organic-free ligands displaying strong affinity towards metal atoms of the chalcogenide nanocrystal surfaces while generating high surface charge is highly desirable to ensure colloidal stabilization required for the preparation of highly pure metal chalcogenide nanocrystal films. S^{2-},[47] $(Sn_2S_6)^{4-}$ molecular metal chalcogenides[17] were recently proposed to replace organic capping ligands on chalcogenide nanocrystals. The ability of a $(Sn_a–Zn_b–S_c)^{t-}$ oligomer solution (x_{Zn} = 0.33) to efficiently strip off SCN^- surface groups from our CZTS nanoparticles synthesized at a high temperature of 400 °C in molten KSCN[27] was demonstrated by infrared spectroscopy (Fig. 10). After making the as-synthesized SCN^--capped CZTS nanoparticles come into contact with $(Sn_a–Zn_b–S_c)^{t-}$ oligomers, complete disappearance of absorption features in IR spectra is observed, confirming the absence of entities containing C–H and N–H bonds. Highly surface charged, perfectly deagglomerated CZTS dispersions were achieved as illustrated by the high electrophoretic mobility up to 5×10^{-4} cm^2 V^{-1} s^{-1} determined on the $(Sn_a–Zn_b–S_c)^{t-}$ oligomer-capped CZTS nanocrystal dispersion as shown in Fig. 10. In spite of the large surface tension of H_2O increasing the capillary stress during film drying, crack-free films with a final thickness of about 1.5–2.5 μm as required for high performance solar cells were successfully prepared from these aqueous nanocrystal dispersions. Fig. 10d depicts a typical 1.5 μm thickness, crack-free film displaying a high green density achieved by deposition of multiple, thin, crack-free layers.

$(Sn_xZn_yS_z)^{t-}$ capped ZnS colloids as composition additives for high performance Cu_2ZnSnS_4 solar cells in an all-aqueous process route. High performance CZTS films require a Cu-poor composition, facilitating the formation of a self-compensated $[V_{Cu}^- + Zn_{Cu}^+]^0$ defect pair.[48] Indeed, CZTS nanocrystals displaying nonstoichiometric compositions are difficult to synthesize, usually yielding ZnS and SnS_2 secondary phases.[49] Fine-tuning of the non-stoichiometric composition of the CZTS film was achieved by infiltration of a $(Sn_a–Zn_b–S_c)^{t-}$ oligomer-capped ZnS colloid aqueous dispersion into the CZTS nanocrystal film. To minimize the chloride contamination of CZTS nanocrystal films, a procedure was developed for the preparation of low-chloride, heterometallic oligomer solutions (section S7†). In order to avoid the formation of cracks arising during film drying, crack-free films were successfully prepared by successive infiltrations into freshly prepared CZTS nanocrystal films. Employing a diluted oligomer solution $(Sn_a–Zn_b–S_c)^{t-}$, x_{Zn} = 0.66 (C_{Zn+Sn} = 0.02 M), fine-tuning of the copper non-stoichiometry with δ(Cu/Zn + Sn) variation as low as 0.02 was achieved as determined by EDS analysis after 6 successive infiltrations onto a 2.2 μm CZTS nanocrystal thick film.

CZTSSe solar cell fabricated from $(Sn_a–Zn_b–S_c)^{t-}$ capped CZTS nanocrystals. Using an all-aqueous $(Sn_a–Zn_b–S_c)^{t-}$-capped CZTS nanocrystal dispersion prepared as described previously, a crack-free CZTS nanocrystal film displaying a thickness of 2.5 μm was successfully prepared under air atmosphere by a multicoating technique onto a glass/Mo electrode. After room temperature drying, the CZTS film (Zn/Sn = 1.3, Cu/(Zn + Sn) = 0.8) was annealed for 15 min under selenium partial pressure (125 mg Se, 15 min) at 580 °C. The sintered CZTSSe films were processed in photovoltaic devices following

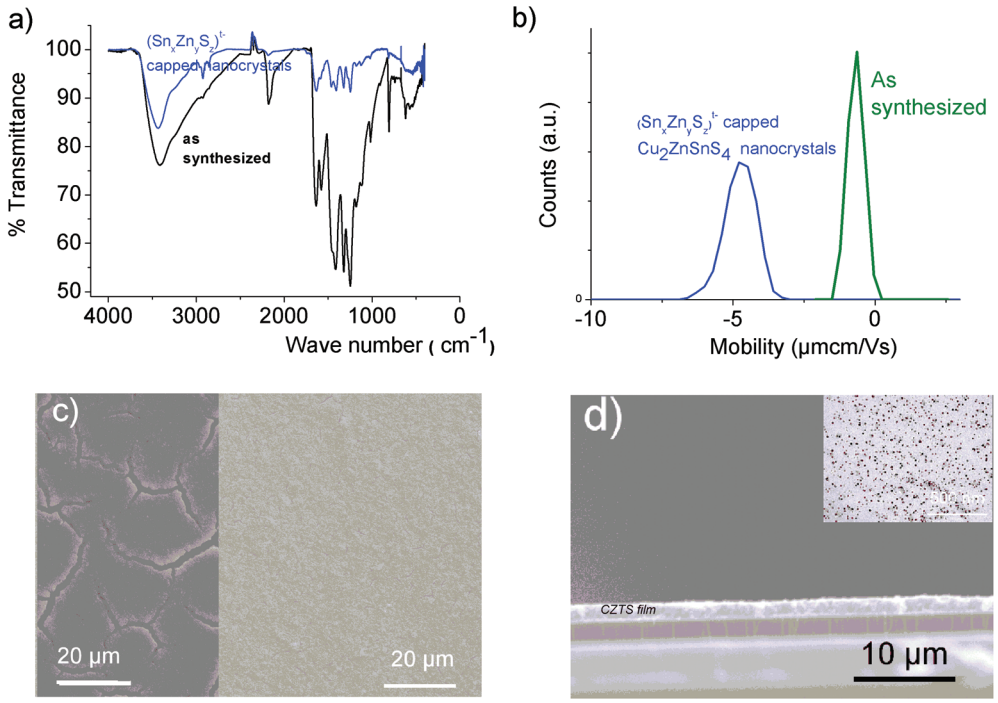

Fig. 10 (a) FTIR spectra of 30 nm, SCN capped (as synthesized) and $(Sn_aZn_bS_c)^t$ oligomers capped Cu_2ZnSnS_4 nanocrystals. (b) Electrophoretic mobility measured for an aqueous solution of 30 nm Cu_2ZnSnS_4 nanocrystals capped with $(Sn_aZn_bS_c)^t$ oligomers. (c) Cu_2ZnSnS_4 nanoparticle film prepared from an aqueous dispersion on the Mo electrode. Left: SEM image of a single coated film reveals the presence of large cracks. Right: SEM image showing a crack free film achieved from oligomer capped CZTS nanocrystals using a multi coating procedure. (d) Typical cross section SEM image of a crack free CZTS film showing a thickness of 1.5 μm. Insert: TEM image of the Cu_2ZnSnS_4 nanocrystal building blocks showing a nano crystal mean diameter of around 30 nm.

standard procedures, including chemical bath deposition of a CdS buffer layer (~50 nm) and RF sputtering of i-ZnO/ZnO:Al. A preliminary conversion efficiency of 2.6% (Fig. S8†) was achieved, demonstrating the efficiency of these heterometallic chalcogenide oligomers as dispersants/ligands to produce environmentally friendly all-aqueous inks for the fabrication of CZTSSe solar cells.

Conclusions

A general synthetic process route under mild conditions is proposed for the preparation of heterometallic chalcogenide oligomers in Sn(IV)–Zn(II)–S(II), Sn(IV)–Zn(II)–Se(II) and Sn(IV)–Ga(III)–S(II) systems. ESI-MS, used as an *in situ* characterization tool, indicates predominant formation of heterometallic oligomers composed of four metal centers in the Sn(IV)–Zn(II)–S(II) and Sn(IV)–Ga(III)–S(II) systems. ^{119}Sn Liquid NMR and Raman experimental data determined on these heterometallic oligomers show a full range of solid solutions achieved for $(Sn_a–Ga_b–S_c)^{t-}$ oligomers, while the incorporation of a sole Zn cation is observed for $(Sn_a–Zn_b–S_c)^{t-}$ oligomers. The heterometallic approach favors the formation of short oligomers, resulting in highly water-soluble species displaying an adamantane structure as shown by the Raman results coupled to quantum chemical calculations. Such low-cost, all-inorganic, environmentally friendly oligomers in association with a residue-free ammonium counterion can potentially be used as chalcogenide precursors in environmentally benign synthetic routes to the formation of electronic grade films. Notably, these heterometallic oligomers represent exciting building blocks for CZTS solar cell fabrication. Indeed, $(Sn_a–Zn_b–S_c)^{t-}$ oligomers, used as dispersants and composition additives, can greatly help in the design of a nontoxic, environmentally friendly, aqueous process route to the fabrication of CZTS absorbers. Using these heterometallic chalcogenide oligomers, a CZTS solar cell has been successfully fabricated with a preliminary device efficiency of 2.6%.

Extension to other systems including Sn(IV)–Ge(IV)–S(II), Sn(IV)–Sb(III)–S(II), and Sn(IV)–Fe(III)–S(II) could open up exciting opportunities for designing new complex chalcogenide materials for applications in electronic devices and thermoelectric materials.

Acknowledgements

This work was mainly supported by funding from the Region Reunion. The authors acknowledge ANR (Agence Nationale de la Recherche, NovACEZ Project) for the development of CZTS solar cells. The authors thank Alain Seraphine for helpful discussions.

References

1 D. B. Mitzi, L. L. Kosbar, C. E. Murray, M. Copel and A. Afzali, *Nature*, 2004, **428**, 299–303.
2 D. K. Kim, Y. Lai, B. T. Diroll, C. B. Murray and C. R. Kagan, *Nat. Commun.*, 2012, **3**, 1216.
3 C. Jiang, J.-S. Lee and D. V. Talapin, *J. Am. Chem. Soc.*, 2012, **134**, 5010–5013.
4 D. Yang, C. Lu, H. Yin and I. P. Herman, *Nanoscale*, 2013, **5**, 7290–7296.
5 M. V. Kovalenko, B. Spokoyny, J.-S. Lee, M. Scheele, A. Weber, S. Perera, D. Landry and D. V. Talapin, *J. Am. Chem. Soc.*, 2010, **132**, 6686–6695.
6 M. Ibáñez, D. Cadavid, R. Zamani, N. García-Castelló, V. Izquierdo-Roca, W. Li, A. Fairbrother, J. D. Prades, A. Shavel, J. Arbiol, A. Pérez-Rodríguez, J. R. Morante and A. Cabot, *Chem. Mater.*, 2012, **24**, 562–570.
7 J. S. Lee, M. V. Kovalenko, J. Huang, D. S. Chung and D. V. Talapin, *Nat. Nanotechnol.*, 2011, **6**, 348–352.
8 D. S. Dolzhnikov, H. Zhang, J. Jang, J. S. Son, M. G. Panthani, T. Shibata, S. Chattopadhyay and D. V. Talapin, *Science*, 2015, **347**, 425–428.
9 H. Li, A. Laine, M. O. Keefe and O. M. Yaghi, *Science*, 1999, **283**, 1145–1147.
10 T. Wu, X. Bu, P. Liao, L. Wang, S.-T. Zheng, R. Ma and P. Feng, *J. Am. Chem. Soc.*, 2012, **134**, 3619–3622.
11 V. B. Krebs, S. Pohl and W. Schiwy, *Z. Anorg. Allg. Chem.*, 1972, **393**, 241–352.
12 W. Schiwy, S. Pohl and B. Krebs, *Z. Anorg. Allg. Chem.*, 1973, **402**, 77–86.
13 S. Pohl, W. Schiwy, N. Weinstock and B. Krebs, *Z. Naturforsch.*, 1973, **28b**, 565–569.
14 B. Krebs, *Angew. Chem., Int. Ed. Engl.*, 1983, **22**, 113–134.
15 B. Krebs, D. Voelker and K. O. Stiller, *Inorg. Chim. Acta*, 1982, **65**, L101–L102.
16 M. V. Kovalenko, M. I. Bodnarchuk, J. Zaumseil, J.-S. Lee and D. V. Talapin, *J. Am. Chem. Soc.*, 2010, **132**, 10085–10092.
17 M. V. Kovalenko, M. Scheele and D. V. Talapin, *Science*, 2009, **324**, 1417–1420.
18 K. Ito and T. Nakazawa, *Jpn. J. Appl. Phys.*, 1988, **27**(11), 2094–2097.
19 H. Katagiri, N. Sasaguchi, S. Hando, S. Hoshino, J. Ohashi and T. Yokota, *Sol. Energy Mater. Sol. Cells*, 1997, **49**, 407–414.
20 Y. S. Lee, T. Gershon, O. Gunawan, T. K. Todorov, T. Gokmen, Y. Virgus and S. Guha, *Adv. Energy Mater.*, 2015, **5**, 1401372.
21 S. Ahmed, K. B. Reuter, O. Gunawan, L. Guo, L. T. Romankiw and H. Deligianni, *Adv. Energy Mater.*, 2012, **2**(2), 253–259.
22 W. Wang, M. T. Winkler, O. Gunawan, T. Gokmen, T. K. Todorov, Y. Zhu and D. B. Mitzi, *Adv. Energy Mater.*, 2013, **1**, 1301465.
23 Y. Cao, M. S. Denny, J. J. Caspar, W. E. Farneth, Q. Guo, A. S. Ionkin, L. K. Johnson, M. Lu, I. Malajovich, D. Radu, H. D. Rosenfeld, K. R. Choudhury and W. Wu, *J. Am. Chem. Soc.*, 2012, **134**(38), 15644–15647.
24 J. V. Embden, A. S. R. Chesman, E. D. Gaspera, N. W. Duffy, S. E. Watkins and J. J. Jasieniak, *J. Am. Chem. Soc.*, 2014, **136**, 5237–5240.
25 G. Larramona, S. Bourdais, A. Jacob, C. Chone, T. Muto, Y. Cuccaro, B. Delatouche, C. Moisan, D. Pere and G. Dennler, *J. Phys. Chem. Lett.*, 2014, **5**, 3763–3767.
26 J. Zhong, Z. Xia, C. Zhang, B. Li, X. Liu, Y. B. Cheng and J. Tang, *Chem. Mater.*, 2014, **26**(11), 3573–3578.
27 J. Y. Chane-Ching, V. Foncrose, O. Zaberca, D. Lagarde, A. Balocchi, X. Marie, T. Blon, P. Puech and R. Bodeux, *Sol. Energy Mater. Sol. Cells*, 2015, **141**, 364–371.
28 A. Carrete, A. Shavel, X. Fontané, J. Montserrat, J. Fan, M. Ibáñez, E. Saucedo, A. Pérez-Rodríguez and A. Cabot, *J. Am. Chem. Soc.*, 2013, **135**(43), 15982–15985.
29 X. Y. Shi, F. Q. Huang, M. L. Liu and L. D. Chen, *Appl. Phys. Lett.*, 2009, **94**, 122103.
30 M. J. Frisch, G. W. Trucks, H. B. Schlegel, G. E. Scuseria, M. A. Robb, J. R. Cheeseman, G. Scalmani, V. Barone, B. Mennucci, G. A. Petersson, H. Nakatsuji, M. Caricato, X. Li, H. P. Hratchian, A. F. Izmaylov, J. Bloino, G. Zheng, J. L. Sonnenberg, M. Hada, M. Ehara, K. Toyota, R. Fukuda, J. Hasegawa, M. Ishida, T. Nakajima, Y. Honda, O. Kitao, H. Nakai, T. Vreven, J. A. Montgomery Jr., J. E. Peralta, F. Ogliaro, M. Bearpark, J. J. Heyd, E. Brothers, K. N. Kudin, V. N. Staroverov, R. Kobayashi, J. Normand, K. Raghavachari, A. Rendell, J. C. Burant, S. S. Iyengar, J. Tomasi, M. Cossi, N. Rega, J. M. Millam, M. Klene, J. E. Knox, J. B. Cross, V. Bakken, C. Adamo, J. Jaramillo, R. Gomperts, R. E. Stratmann, O. Yazyev, A. J. Austin, R. Cammi, C. Pomelli, J. W. Ochterski, R. L. Martin, K. Morokuma, V. G. Zakrzewski, G. A. Voth, P. Salvador, J. J. Dannenberg, S. Dapprich, A. D. Daniels, Ö. Farkas, J. B. Foresman, J. V. Ortiz, J. Cioslowski and D. J. Fox, Gaussian, Inc., Wallingford CT, 2009.
31 J. P. Perdew, J. A. Chevary, S. H. Vosko, K. A. Jackson, M. R. Pederson, D. J. Singh and C. Fiolhais, *Phys. Rev. B: Condens. Matter*, 1992, **46**, 6671–6687.
32 A. D. Becke, *J. Chem. Phys.*, 1993, **98**, 5648–5652.
33 A. Bergner, M. Dolg, W. Kuechle, H. Stoll and H. Preuss, *Mol. Phys.*, 1993, **80**, 1431–1441.
34 M. Dolg, U. Wedig, H. Stoll and H. Preuss, *J. Chem. Phys.*, 1987, **86**, 866–872.
35 T. Leininger, A. Berning, A. Nicklass, H. Stoll, H.-J. Werner and H.-J. Flad, *Chem. Phys.*, 1997, **217**, 19–27.
36 J. M. L. Martin and A. Sundermann, *J. Chem. Phys.*, 2001, **114**, 3408–3420.
37 A. D. McLean and G. S. Chandler, *J. Chem. Phys.*, 1980, **72**, 5639–5646.
38 A. V. Marenich, C. J. Cramer and D. G. Truhlar, *J. Phys. Chem. B*, 2009, **113**, 6378–6396.
39 X. Bu, N. Zheng and P. Feng, *Chem. – Eur. J.*, 2004, **10**, 3356–3362.
40 B. R. Tagirov, O. M. Suleimenov and T. M. Seward, *Geochim. Cosmochim. Acta*, 2007, **71**, 4942–4953.

41 Z. Y. Xu and Y. C. Zhang, *Mater. Chem. Phys.*, 2008, **112**, 333–336.
42 O. Brafman and S. S. Mitra, *Phys. Rev.*, 1968, **171**, 931–934.
43 J. Campbell, D. P. Diciommo, H. P. A. Mercier, A. M. Pirani, G. J. Schrobilgen and M. Willuhn, *Inorg. Chem.*, 1995, **34**, 6265–6272.
44 S. M. Shapiro and J. D. Axe, *Phys. Rev. B: Condens. Matter*, 1972, **6**, 2420.
45 G. Landa, R. Carles and J. B. Renucci, *Solid State Commun.*, 1993, **86**, 351–355.
46 F. Lips and S. Dehnen, *Inorg. Chem.*, 2008, **47**, 5561–5563.
47 A. Nag, M. V. Kovalenko, J. S. Lee, W. Liu, B. Spokoyny and D. V. Talapin, *J. Am. Chem. Soc.*, 2011, **133**, 10612–10621.
48 S. Chen, X. G. Gong, A. Walsh and S. H. Wei, *Appl. Phys. Lett.*, 2010, **96**, 021902–021903.
49 L. Choubrac, A. Lafond, C. Guillot-Deudon, Y. Moelo and S. Jobic, *Inorg. Chem.*, 2012, **51**(6), 3346–3348.

Electronic Supplementary Material (ESI) for Inorganic Chemistry Frontiers.

Supporting information

Heterometallic chalcogenide oligomers as building blocks for an environmentally-friendly, low-cost, solar cells fabrication.

J.Y. Chane-Ching,[a*] L. Perrin,[b] P. Puech,[c] V. Bourdon,[d] V. Foncrose,[a] A. Balocchi,[e] X. Marie,[e] P. Lavedan[d]

[a]Université de Toulouse, UPS, CNRS, CIRIMAT, 118 Route de Narbonne, F-31062, Toulouse
[b]Université de Lyon 1, ICBMS, CNRS, INSA, CPE 43 Bd du 11 nov 1918, 69622 Villeurbanne cedex
[c]Université de Toulouse, CNRS, CEMES, 29 rue Jeanne Marvig 31055 Toulouse, France.
[d]Université de Toulouse, UPS, Service commun, 118 Route de Narbonne, F-31062, Toulouse
[e]Université de Toulouse, INSA-CNRS-UPS, LPCNO, 135 Av. Rangueil, 31077 Toulouse, France.

Email address: chane@chimie.ups-tlse.fr

Table of contents

S1- h- s oligomers formation domains.

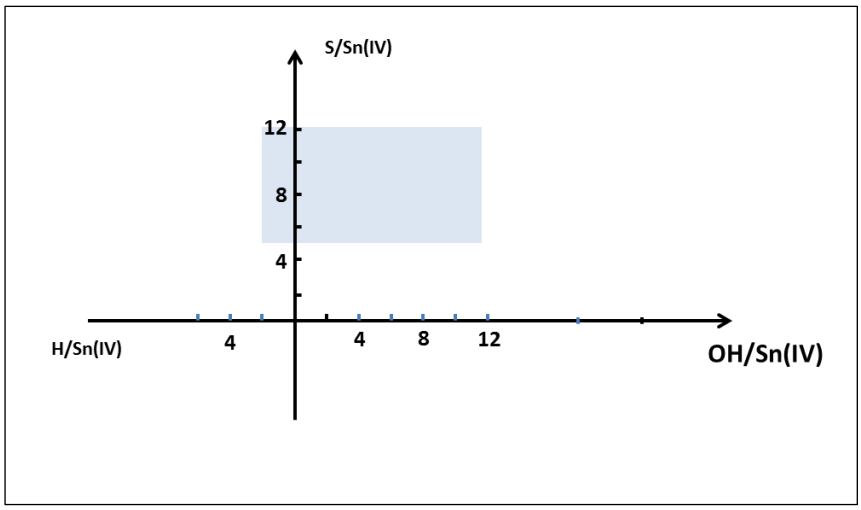

Figure S1a. h-s $(Sn_a–S_c)^{t-}$ oligomers formation domain. s denotes $[S^{2-}]/[Sn^{4+}]$ molar ratio and h = [H]/ $([Sn^{4+}])$ or [OH]/$([Sn^{4+}])$ molar ratios. [H], [OH] being the molar concentration in the metallic solution. The h-s formation domain is determined at $^{-}[Sn^{4+}]$ = 0.1M. Blue area depicts the as-synthesized limpid solutions.

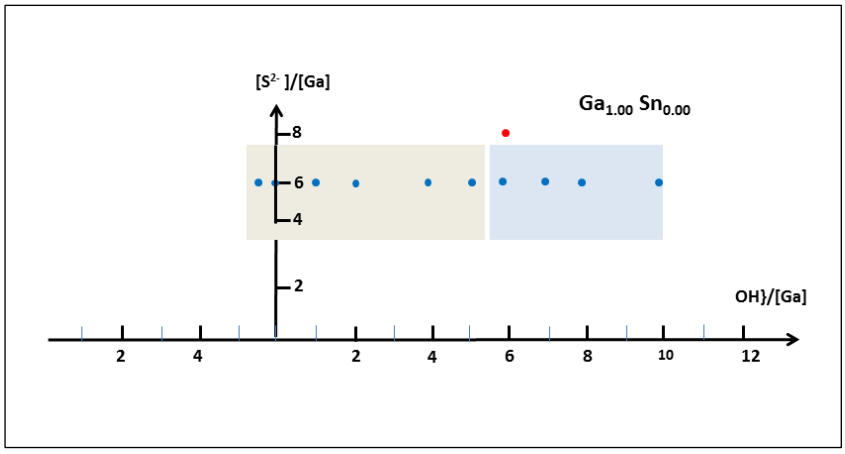

Figure S1b. Figure S1b: h-s $(Ga_a–S_c)^{t-}$ oligomers formation domain. s denotes $[S^{2-}]/[Ga^{3+}]$ molar ratio and h = [H]/ $([Ga^{3+}])$ or [OH]/$([Ga^{3+}])$ molar ratios. [H], [OH] being the molar concentration in the metallic solution. The h-s formation domain is determined at $^{-}[Ga^{3+}]$ = 0.1 M. The colored areas depict the domain of limpid oligomer solutions. Blue area: as-synthesized limpid solutions. Grey area: limpid solutions in low ionic strength conditions

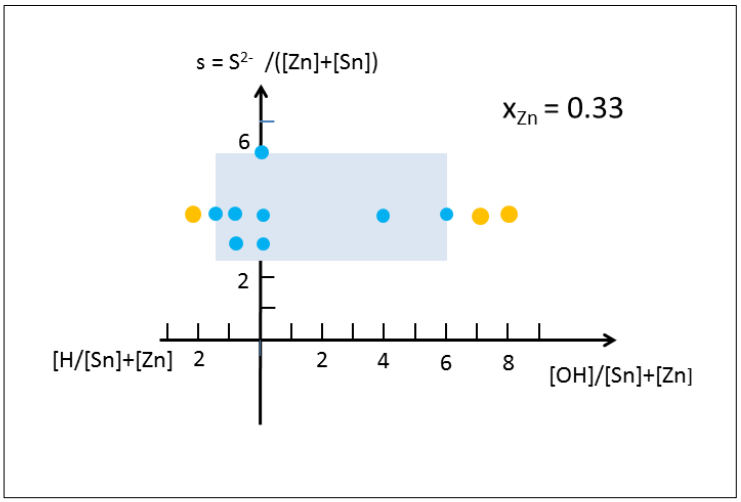

Figure S1c. Typical $(Sn_a–Zn_b–S_c)^{t-}$ oligomers formation domain, x_{Zn}= 0.33. s denotes $[S^{2-}]/[Sn^{4+}]+[Zn^{2+}]$ molar ratio and h = [H]/ $([Sn^{4+}]+[Zn^{2+}])$ or $[OH]/([Sn^{4+}]+[Zn^{2+}])$. [H], [OH] being the molar concentration in the metallic solution. Total metal concentration of the reaction mixtures is 0.1 M. The blue area represents the oligomer formation domain. pH values were ranging from 8.6 ([H]/[Sn]+[Zn] = 1.5) to 11.6 ([OH]/[Zn]+[Sn] = 6).

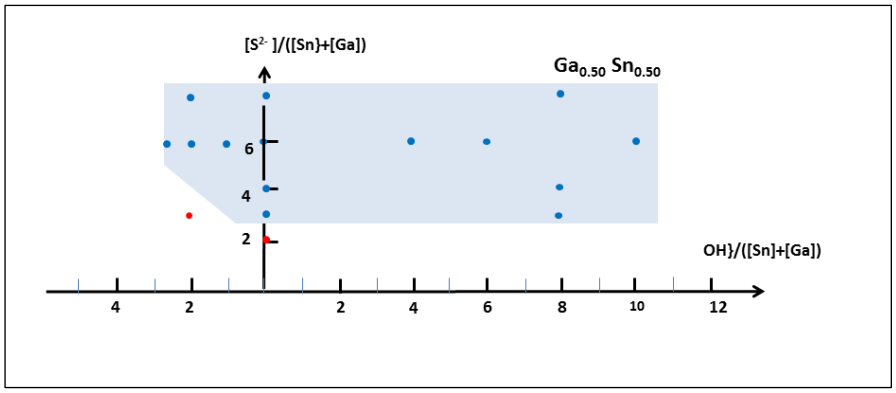

Figure S1d. Typical $(Sn_a–Ga_b–S_c)^{t-}$ oligomer formation domain, x_{Ga}= 0.5, showing successful preparation of limpid dispersions in a large range of [OH]/ ([Sn]+[Ga]) values, ([Sn]+[Ga]) = 0.1 M.

S2- ESI-MS spectrum of $(Sn_a–S_c)^{t-}$ prepared in highly basic pH

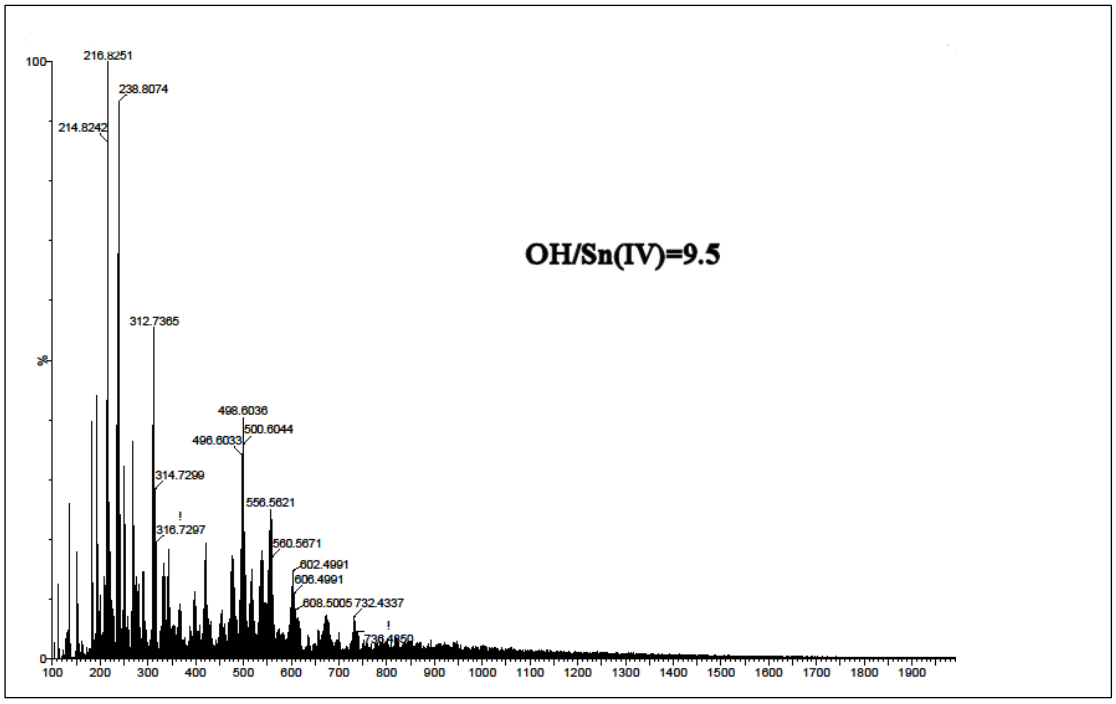

Figure S2. Negative ion ESI-MS experimental spectrum of $(Sn_aZn_bS_c)^{t-}$ oligomer, x $_{Zn}$=0, Sn(IV)= 0.1M and OH/Sn= 9.5 molar. The OH/Sn ratio was adjusted using NaOH. We can observe m/z= 398.4 $(Sn_2S_5H)^-$, m/z= 420.4 $(Sn_2S_5Na)^-$ m/z= 581 $(Sn_3S_7H)^-$, m/z= 602.5 $(Sn_3S_7Na)^-$. On can note that $(Sn_4S_{10}H_3)^-$ tetramers m/z= 798.3 are not observed in highly basic conditions.

S3- Confirmation of chemical composition. Comparison of ESI-MS experimental isotopic distribution with theoretical spectra.

S3-1- Monometallic oligomers

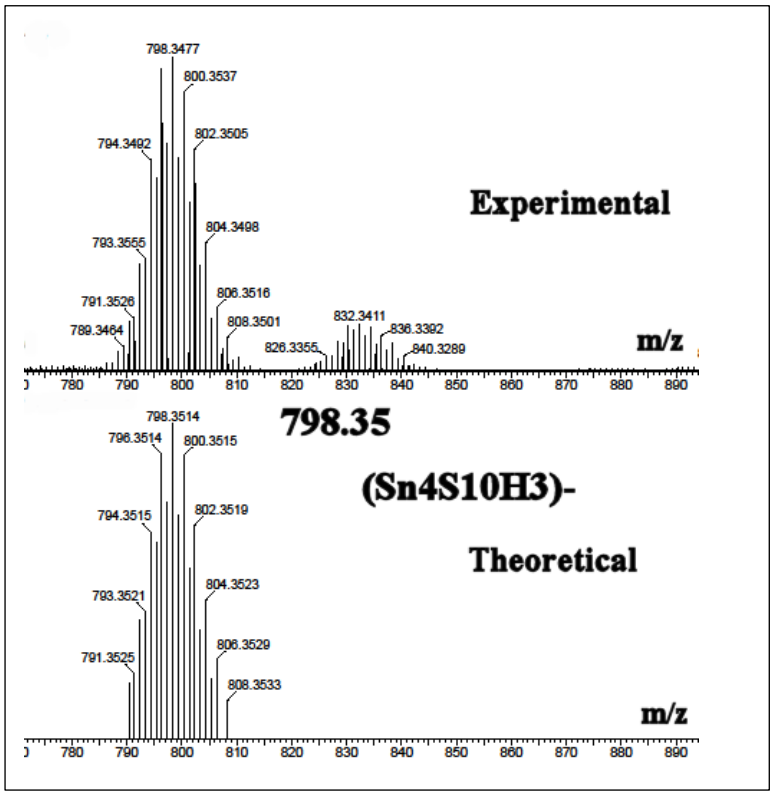

Figure S3a. Confirmation of chemical composition for m/z= 798.35 $(Sn_4S_{10}H_3)^-$, detected by ESI-MS.

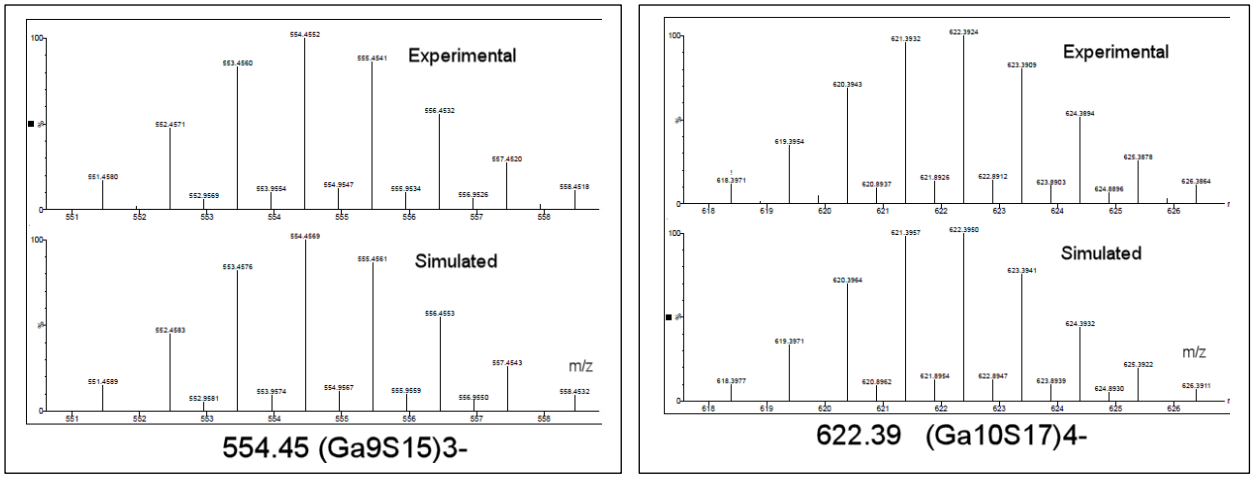

Figure S3b. Confirmation of chemical composition (A) for m/z= 554.45 $(Ga_9S_{15})^{3-}$, (B) for m/z= 622.39 $(Ga_{10}S_{17})^{4-}$, detected by ESI-MS.

3-2-($Sn_aZn_bS_c)^{t-}$ et ($Sn_aZn_bSe_c)^{t-}$ oligomers.

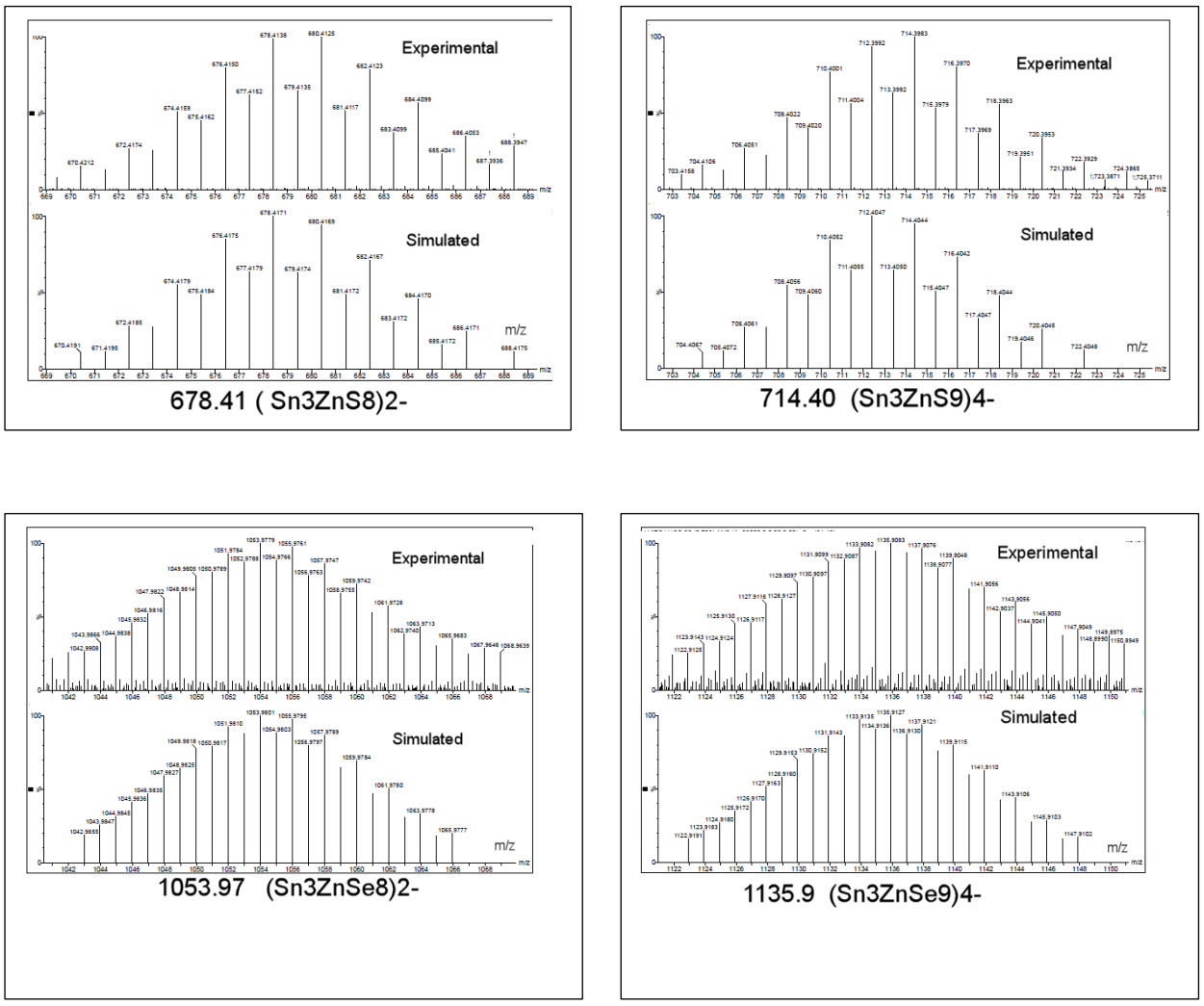

Figure S3c. Confirmation of chemical composition (A) for m/z = 678.41 $(Sn_3\ Zn_1S_8)^{2-}$, (B) for m/z = 714.40 $(Sn_3\ Zn_1S_9)^{4-}$ (C) for m/z = 1053.97 $(Sn_3\ Zn_1Se_8)^{2-}$, (D) for m/z = 1135.9$(Sn_3\ Zn_1Se_9)^{4-}$detected by ESI-MS.

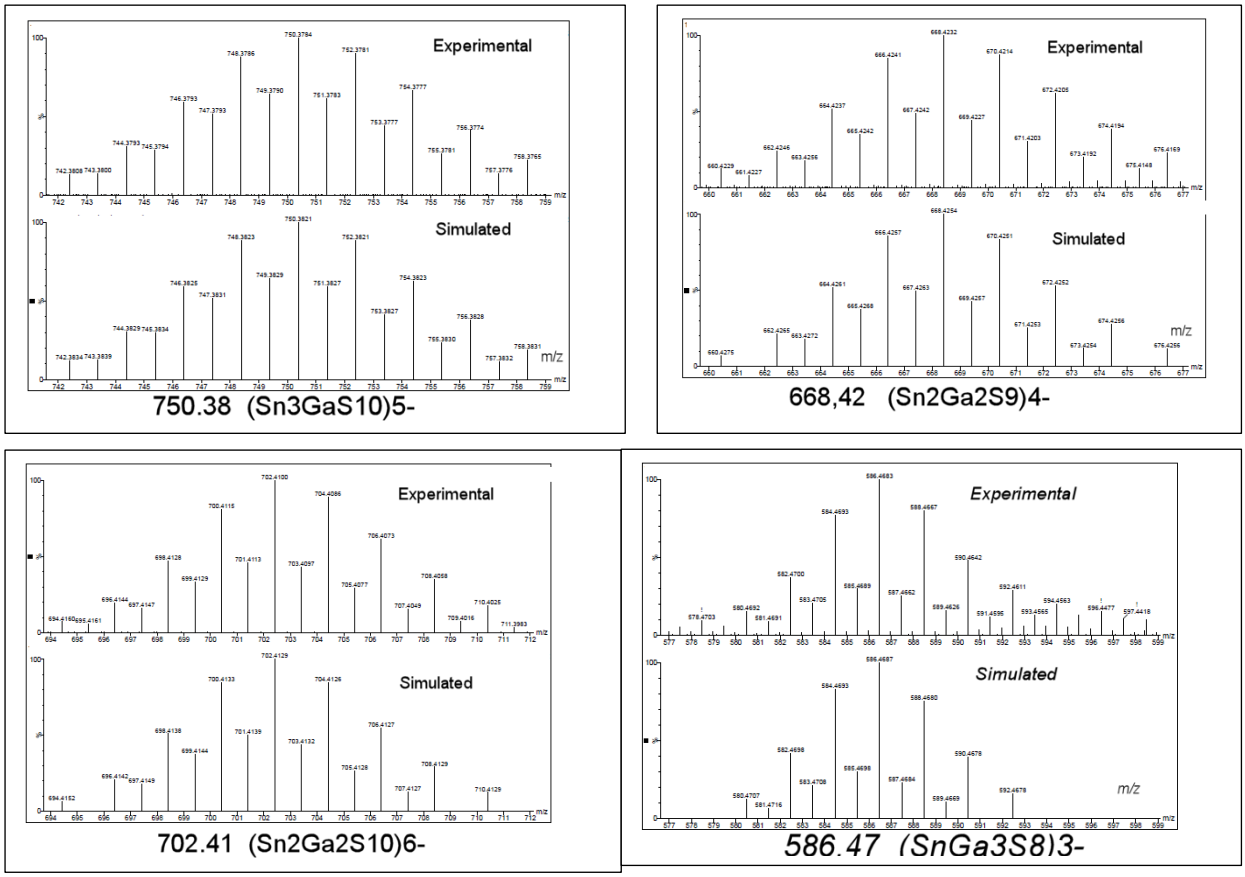

Figure S3d. Confirmation of chemical composition (A) for m/z = 750.38 $(Sn_3\ Ga_1S_{10})^{5-}$, (B) for m/z = 668.42 $(Sn_2\ Ga_2S_9)^{4-}$ (C) for m/z = 702.41 $(Sn_2\ Ga_2S_{10})^{6-}$, (D) for m/z = 586.47 $(Sn\ Ga_3S_8)^{3-}$detected by ESI-MS.

S4- $(Sn_a–Zn_b–S_c)^{t-}$ oligomers-capped ZnS colloids

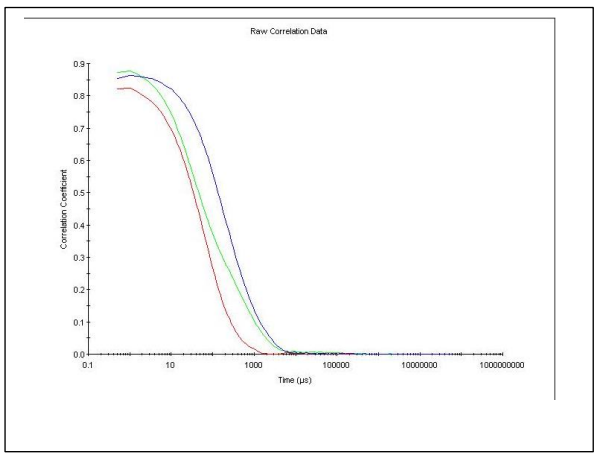

Figure S4. Correlogramms recorded by dynamic light scattering on Sn(IV)-Zn(II)-S dispersions showing monodisperse size distribution for $0.2 < x_{Zn} < 0.50$ and an increase

average hydrodynamic diameter with x_{Zn}. Corresponding hydrodynamic diameters of 4.25 nm, 5.5 nm and 18.5 nm were respectively determined for x_{Zn}= 0.5 (s= 6, red curve) x_{Zn}= 0.66 (s= 4, green curve) x_{Zn}= 0.66 (s= 6, Blue curve).

S5- DFT results.

Oligomers	Frequency, cm^{-1} (Raman Scattering Activity >20 $a^4.amu^{-1}$)
$(Sn_4S_{10})^{4-}$	70.4(22) 72.6(22) 96.7(33) 98.4(34) 99.0(32) 133.0(99) 287.2(88) **287.7**(318) **289.5**(63) 301.2(29) 302.9(26) **338.8**(46) **339.4**(47) **340.5**(47) **386.0**(92) **386.5**(92) **387.0**(88) **393.9**(408) Main peak: **390**
*$(Sn_3GaS_{10})^{5-}$	74.3(22) 98.9(23) 99.8(29) 108.5(32) **140.6**(74) 274.2(34) **287.6**(315) 292.2(33) 293.9(47) 321.5(35) 324.0(40) **350.8**(375) **372.8**(113) **375.4**(102) **377.0**(204) **388.2**(151) Main peak: **372**
*$(Sn_2Ga_2S_{10})^{6-}$	105.2(32) 147.0(63) 272.3(52) **279.1**(57) **281.9**(118) **298.0**(70) 303.7(32) 327.9(27) 330.3(38) **337.8**(387) 351.1(91) **359.6**(120) **361.3**(210) **374.3**(106) Main peak **343**
$(SnGa_3S_{10})^{7-}$	100.7(22) **148.9**(57) 258.9(21) **277.6**(118) 294.6(45) **325.6**(355) **330.3**(98) **333.2**(88) **341.0**(138) **349.4**(63) 353.4(57) Main peak: **329**
$(Ga_4S_{10})^{8-}$	151.9(58) 267.2(27) 277.8(45) **280.7**(110) 295.2(21) 310.1(55) **312.7**(78) **314.8**(68) 330.0(32) 330.7(76) Main peak: **310**

Table S5. Calculated Raman shift and scattering activities of $(Sn_aGa_bS_c)^{t-}$ adamantane –like structures. * denote oligomers observed by mass spectrometry. The frequency of main peak has been determined by convoluting Lorentzian functions whose amplitudes are proportional to computed Raman activity intensities and a half-band width of 20 cm^{-1}. Increase of the number of substituted Ga cations into the adamantane-like structure clearly results in a decrease of the frequency of the Raman main peak.

Cartesian Coordinates of DFT-Optimized Compounds and There Related Energies. 8

$[SnSe_3]^{2-}$

4
scf done: -31.991577

Sn	0.490921	-0.248044	-0.371230
Se	2.665337	-0.086782	0.764849
Se	-0.673701	-2.409616	-0.493915
Se	-0.519382	1.752668	-1.382976

$[SnSe_4]^{4-}$

5
scf done: -41.679006

Sn	0.301056	-0.119670	0.178351
Se	-0.726686	0.404852	2.464426
Se	2.854166	-0.179276	0.384191
Se	-0.534169	-2.404561	-0.628920
Se	-0.386572	1.684144	-1.503468

$[Sn_2Se_5]^{2-}$

12
scf done: -3423.503759

Zn	0.035128	-0.286652	-0.477250
S	2.229832	0.321887	-0.811671
S	-0.952851	-2.353384	-0.739872
S	-1.600291	1.571050	-0.925008
Sn	2.313362	0.145488	-3.212983
Sn	-0.815405	-2.556558	-3.137441
Sn	-1.273261	1.134293	-3.174278
S	4.335352	0.635105	-4.208283
S	0.698452	1.900482	-4.221145
S	-1.607630	-4.516353	-4.057786
S	1.425335	-2.009264	-4.020390
S	-2.332433	-0.725598	-4.171111

lin-$[Sn_4Se_{10}]^{4-}$

14
scf done: -108.676640

Sn	0.072410	-0.194489	-0.198413
Se	-0.621784	0.367216	2.323374
Se	2.679248	-0.169226	0.404535
Se	-0.653946	-2.490249	-0.802350
Se	-0.490592	1.707229	-1.691116
Sn	1.881709	0.351512	2.761370
Se	2.850891	2.490727	3.839126
Se	2.692145	-1.263953	4.609212

Sn	3.661303	0.875266	5.686982
Se	2.863717	1.396005	8.043802
Se	6.164787	0.859571	6.125023
Sn	5.470544	1.421292	8.646794
Se	6.033535	-0.480410	10.139521
Se	6.196875	3.717062	9.250724

ada-$[Sn_4Se_{10}]_{4-}$

14
scf done: -108.694776

Sn	-0.045393	-0.196485	0.035593
Se	-0.042109	-0.122814	2.509769
Se	2.370392	0.244251	-0.775517
Se	-0.850539	-2.540276	-0.699554
Se	-1.654386	1.639547	-0.815407
Sn	2.307541	0.158294	-3.358562
Sn	-0.831520	-2.548833	-3.285153
Sn	-1.610370	1.523236	-3.398117
Se	4.598545	0.573143	-4.199431
Se	0.764593	2.008064	-4.300225
Se	-1.603016	-4.774766	-4.045891
Se	1.562830	-2.174962	-4.187928
Se	-3.132941	3.269215	-4.270786
Se	-2.458141	-0.773759	-4.230101

ada-$[Sn_3ZnSe_9]^{4-}$

13
scf done: -323.075542

Zn	-0.026327	-0.218036	-0.582476
Se	2.391762	0.260094	-0.683679
Se	-0.846429	-2.547937	-0.600183
Se	-1.689017	1.621990	-0.725405
Sn	2.336592	0.169684	-3.221688
Sn	-0.846383	-2.569038	-3.140102
Sn	-1.634335	1.552683	-3.260409
Se	4.564965	0.555783	-4.269535
Se	0.757716	1.998328	-4.195419
Se	-1.599263	-4.738968	-4.108279
Se	1.544353	-2.154260	-4.090127
Se	-3.103054	3.247253	-4.347079
Se	-2.430792	-0.764000	-4.149377

ada-$[Sn_3Zn_2Se_8]^{4-}$

12
scf done: -537.441905

Zn	-0.108019	-0.394546	-0.590756	10
Se	2.334172	0.184271	-0.748642	
Se	-0.894929	-2.694482	-0.563477	
Se	-1.666603	1.576438	-0.777666	
Sn	2.328744	0.077750	-3.302088	
Zn	-0.616565	-1.916775	-2.861563	
Sn	-1.684989	1.470255	-3.331981	
Se	4.579428	0.644031	-4.251431	
Se	0.734367	1.937715	-4.240725	
Se	1.526210	-2.204890	-4.112203	
Se	-3.065491	3.303781	-4.340378	
Se	-2.447274	-0.831005	-4.144570	

ada-$[Sn_4S_{10}]^{4-}$

14

scf done: -3996.440783

Sn	-0.045571	-0.197010	-0.037223
S	-0.043359	-0.134519	2.282352
S	2.230653	0.202809	-0.876754
S	-0.809341	-2.405273	-0.802876
S	-1.548658	1.540028	-0.915683
Sn	2.238132	0.148943	-3.333293
Sn	-0.808434	-2.486001	-3.260757
Sn	-1.564648	1.469116	-3.375210
S	4.385564	0.542027	-4.119568
S	0.718189	1.878043	-4.193990
S	-1.530426	-4.571688	-3.976479
S	1.466521	-2.058404	-4.093282
S	-2.992447	3.104519	-4.195710
S	-2.320688	-0.748736	-4.122837

lin-$[Sn_4S_{10}]^{4-}$

14

scf done: -3996.415696

Sn	0.155596	-0.167751	-0.060806
S	-0.448613	0.386829	2.397748
S	2.661039	-0.113633	0.595367
S	-0.492176	-2.348647	-0.556529
S	-0.339933	1.646592	-1.433553
Sn	1.905546	0.369671	2.809935
S	2.841309	2.372838	3.876938
S	2.701807	-1.146047	4.571345
Sn	3.637521	0.857128	5.638377
S	2.881917	1.340431	7.852908
S	5.991659	0.839999	6.050677
Sn	5.387321	1.394540	8.509212
S	5.882790	-0.419823	9.881952

S	6.035060	3.575427	9.005013	11

ada-$[Ga_4S_{10}]^{8-}$

14
scf done: -4289.678285

Ga	-0.048278	-0.199922	-0.145783
S	-0.054905	-0.141517	2.154112
S	2.141572	0.197329	-0.945958
S	-0.771605	-2.330249	-0.865324
S	-1.517591	1.461282	-0.968514
Ga	2.137752	0.126645	-3.308676
Ga	-0.771182	-2.390024	-3.226804
Ga	-1.495285	1.408863	-3.333297
S	4.270751	0.497995	-4.092348
S	0.698386	1.821816	-4.126460
S	-1.500104	-4.461899	-3.911871
S	1.420916	-2.009943	-4.024927
S	-2.938501	3.018885	-4.127960
S	-2.196441	-0.715407	-4.097499

lin-$[Ga_4S_{10}]^{8-}$

14
scf done: -4289.688653

Ga	0.318252	-0.121248	0.143820
S	-0.368930	0.381423	2.440665
S	2.676240	-0.148305	0.785876
S	-0.410283	-2.192581	-0.538369
S	-0.146887	1.623550	-1.275987
Ga	1.903319	0.351485	2.914798
S	2.772330	2.298780	3.919606
S	2.628682	-1.104489	4.622407
Ga	3.551458	0.835839	5.593632
S	2.888467	1.288420	7.769466
S	5.844862	0.843149	5.944535
Ga	5.279313	1.363529	8.265452
S	5.913362	-0.309381	9.702483
S	5.950658	3.477385	8.850199

ada-$[Sn_3GaS_{10}]^{5-}$

14
scf done: -4069.772394

Ga	-0.044505	-0.197220	-0.054129
S	-0.060936	-0.135415	2.167095
S	2.154278	0.197562	-0.862551
S	-0.765354	-2.335639	-0.789762
S	-1.502419	1.476384	-0.896406
Sn	2.224056	0.145687	-3.278747

Sn	-0.801077	-2.472845	-3.203963	12
Sn	-1.555729	1.462848	-3.314713	
S	4.368609	0.535689	-4.127189	
S	0.711045	1.857243	-4.219975	
S	-1.530305	-4.555076	-3.980774	
S	1.456577	-2.048429	-4.121530	
S	-2.976341	3.099144	-4.197472	
S	-2.302412	-0.746077	-4.141194	

ada-$[Sn_2Ga_2S_{10}]^{6-}$

14
scf done: -4143.088763

Ga	0.003219	-0.187702	-0.086636
S	-0.068826	-0.141748	2.157065
S	2.130449	0.202744	-0.950363
S	-0.789343	-2.335521	-0.788285
S	-1.532111	1.462330	-0.895661
Ga	2.212393	0.146276	-3.276082
Sn	-0.750248	-2.453037	-3.214775
Sn	-1.497326	1.462030	-3.325666
S	4.276518	0.505476	-4.090434
S	0.748743	1.808991	-4.186581
S	-1.526651	-4.547493	-3.977917
S	1.467274	-1.979334	-4.088081
S	-2.970596	3.091084	-4.190593
S	-2.328008	-0.750241	-4.107300

ada-$[SnGa3S_{10}]^{7-}$

14
scf done: -4216.390241

Sn	-0.041044	-0.199942	-0.125233
S	-0.028077	-0.139940	2.257084
S	2.222078	0.212197	-0.941285
S	-0.813247	-2.390412	-0.874442
S	-1.559516	1.509799	-0.981879
Ga	2.145975	0.130566	-3.357426
Ga	-0.783706	-2.399588	-3.289969
Ga	-1.503685	1.407879	-3.399426
S	4.267447	0.500555	-4.082329
S	0.699740	1.828519	-4.091419
S	-1.493000	-4.467480	-3.911495
S	1.413102	-2.001511	-4.002732
S	-2.931792	3.015111	-4.141405
S	-2.218788	-0.721897	-4.079354

S6- TGA and XRD obtained after thermal decomposition of the hetero-metallic chalcogenide oligomers. 13

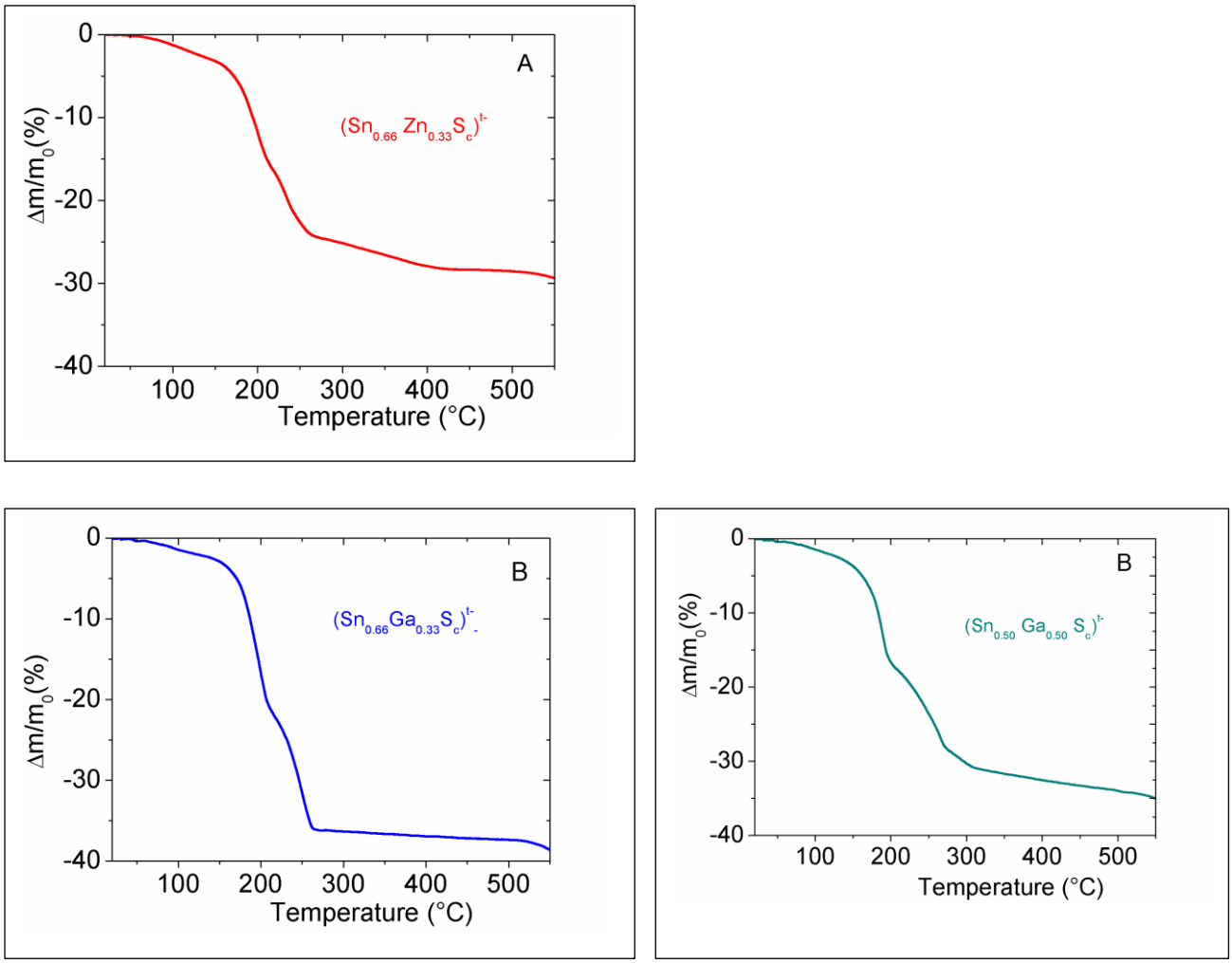

Figure S6-a: TGA curves recorded on (A): NH_4Cl-$(NH_4)_2S$-$(Sn_aZn_bS_c)^{t-}$ and (B): NH_4Cl-$(NH_4)_2S$-$(Sn_aGa_bS_c)^{t-}$ solid samples showing two decomposition temperatures occurring at T< 250 °C. $(Sn_aZn_bS_c)^{t-}$ oligomers were prepared at x_{Zn}= 0.33, ([Zn]+[Sn])= 0.2M, s= $(NH_4)_2S$/([Sn]+[Sn])= 6). $(Sn_aGa_bS_c)^{t-}$ oligomers were synthesized at x_{Ga}= 0.33 (Sn+Ga= 0.40M, s= 6) and x_{Ga}= 0.50 (Sn+Ga= 0.35M, s= 6). The solid samples were collected after evaporating the oligomer solutions at room temperature during 16 h, centrifugation at 4500 rpm, 10 min and drying at 30 °C under air atmosphere. TGA curves were recorded under N_2 at heating rate v= 0.5 °C min^{-1}.

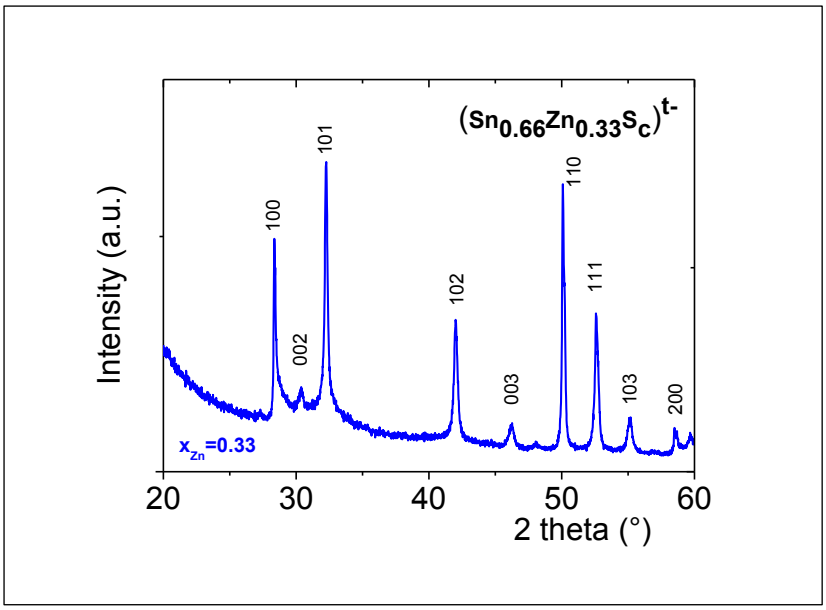

Fig S6-b: X-ray diffractogram recorded on $(Sn_aZn_bS_c)^{t-}$, x_{Zn}= 0.33 solid oligomer after calcination at 550 °C 2h under N_2. Decomposition into the parent metal chalcogenides is observed resulting for x_{Zn}=0.33 in the formation of a SnS_2 solid solution (Hexagonal , 00-022-0951).

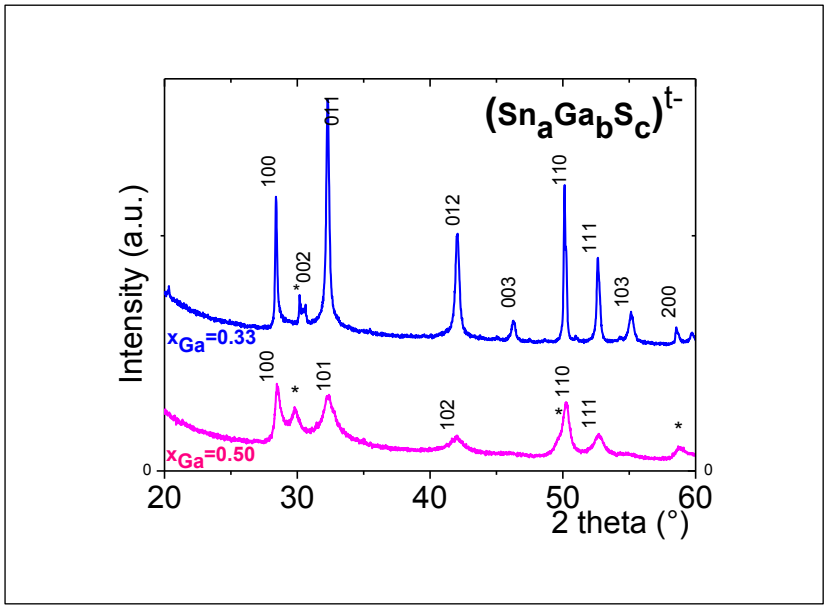

Fig S6-c: X-ray diffractogram recorded on $(Sn_aGa_bS_c)^{t-}$, x_{Ga} = 0.33 and x_{Ga}= 0.55 solid oligomers after calcination at 550 °C 2h under N_2. $Sn_{1,x}Ga_xS_2$ solid solution (SnS_2 Hexagonal, 01-089-2358) and trace of Ga_2S_3 (Cubic, 03-065-7839) are observed for the sample prepared at x_{Ga}= 0.33 while Ga_2S_3 (Cubic, 00-043-0916) and SnS_2 (Hexagonal, 00-040-1467) structures are identified at x_{Ga}= 0.50. Note the better crystallization of the sample prepared at x_{Ga}= 0.33.

S7- Low-chloride hetero-metallic oligomers solutions preparation for infiltration **15**

The $(Sn_a–Zn_b–S_c)^{t-}$ hetero-metallic oligomers were used as composition additives to fine tune the Cu non stoichiometry of CZTS nanocrystals films. To avoid chloride contamination of CZTS nanocrystals films, a procedure was developed for the synthesis of low-chloride hetero-metallic oligomers solutions. Oligomer solutions with concentration close to the solubility limit as indicated in the oligomers formation domain were prepared. Room-temperature evaporation under stirring of these solutions yields super-saturated oligomers solutions which precipitate with time (t= 16 h). The solid precipitate was isolated and re-dispersed in a diluted $(NH_4)_2S$ solution producing low chloride oligomer solutions displaying total metal cations concentration larger than 0.5 M. In a typical synthesis, a 0.2 M solution of $(Sn_a–Zn_b–S_c)^{t-}$, x_{Zn}= 0.33, oligomers are prepared at 0.2 M ([Sn]+[Zn]). The oligomer solution is evaporated at room temperature overnight under stirring. The solid precipitate (4.16 g) is isolated by centrifugation at 4500 rpm. The $(Sn_a–Zn_b–S_c)^{t-}$ oligomer solution is obtained by re-dissolution in 0.02 M $(NH_4)_2S$ solution.

S8- Solar cells characteristics

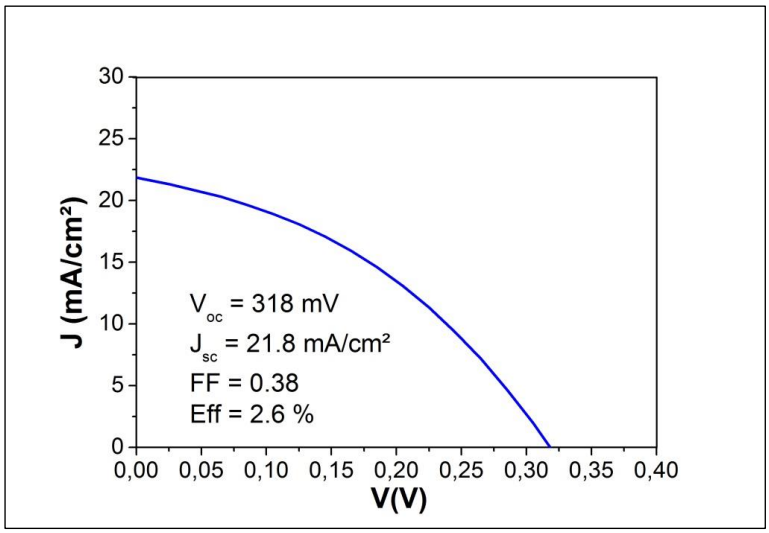

Figure S8. Current voltage curve and solar cell characteristics for the Mo/CZTSSe/CdS/ ZnO: ZnO/Al cell.